

UNIVERSITY OF OSLO
Department of
Geosciences

**Is there a positive
feedback between
Arctic stratus and
Arctic sea ice
changes?**

Master thesis in
Geosciences
Meteorology and
oceanography

Mari Fenn
Kristiansen

1st June 2015



*Rows and flows of angel hair
and ice cream castles in the air
and feather canyons
everywhere,
I've looked at clouds that way.*

JONI MITCHELL

Abstract

This will be my abstract.

Write it later....

No more than a page and should contain:

- main findings - how it compares to others - a conclusion?

Acknowledgements

First of all I want to thank my main supervisor Jón Egill Kristjánsson for an interesting project and for the opportunity to come and work at NCAR for a couple of weeks. I also want to thank my other supervisor Kari Alterskær for her "poking" and setting deadlines and pushing me for the past few months. I greatly appreciate their guidance and criticism throughout this project, and the doors that were always safe to knock on.

Thank you so much to Anne Claire Fullioux for helping me with setting up and getting started with WRF, and to both her and Kjell Andresen for help with technical problems during my work with this thesis. Thanks should also be given to Kjetil Schanke Aas for always taking time to answer any stupid WRF-related questions I might have had.

Thanks also to Gregory Thompson whom Jón Egill and I met with in Boulder, for meeting with us and answering all my e-mails about running the new aerosol-aware microphysics scheme in WRF.

These past two years have been very enjoyable in all their stress thanks to Marta and Helle especially, for all their positiveness.

Last, but not least, I would like to thank Henrik Andersen Sveinsson, for great technical help, but mostly for bearing with me through the last few weeks – it can't have been easy.

Contents

1	Introduction	9
1.1	Main goal	10
1.2	My contribution	11
1.3	Area description	11
1.4	Background	12
1.5	Structure of the thesis	13
2	Theory of Clouds and Radiation	15
2.1	Cloud effects on radiation	15
2.1.1	The Cloud – a gray body	15
2.1.2	Cloud optical depth	16
2.1.3	Cloud albedo	17
2.1.4	Cloud droplet effective radius	17
2.1.5	Liquid water content and path	18
2.1.6	Ice water path	21
2.2	Aerosols and clouds	21
2.2.1	The first indirect effect	22
2.2.2	The second indirect effect	23
2.3	Arctic clouds	24
3	Model and methods	27
3.1	Description of the WRF-ARW Modeling System	27
3.2	Model setup	31
3.2.1	Choices of physics in the model	32
3.3	Model runs	35
3.3.1	Input data	36
3.3.2	Manipulation of input files	36
3.4	Processing of the results	36
4	Results and discussion	39
4.1	The control run	39
4.2	Removed sea ice	41
4.2.1	Day 1	41

4.2.2	Day 5	43
4.3	Increased aerosol concentration	45
4.3.1	Day 1	45
4.3.2	Day 5	46
5	Summary and Conclusions	61

Chapter 1

Introduction

Since 1979, the areal extent of Arctic sea ice in early autumn has shrunk by 80% according to satellite data (cite@ NSIDC). According to satellite data, the decline appears to be particularly rapid after 2000 [Wu & Lee, 2012].

Since 1979, the areal extent of Arctic sea ice in early autumn has shrunk by 80%, according to satellite data (e.g. National Snow and Ice Data Center, U.S.A.). The decline appears to be particularly rapid after 2000, as documented by new satellite data sets (Wu and Lee, 2012). The dramatic reduction in sea ice extent may have contributed strongly to the rapid warming of the Arctic observed in recent years, due to increased fluxes of sensible and latent heat from the Arctic Ocean to the overlying atmosphere (Screen and Simmonds, 2010). Other factors may also contribute such as changes in the atmospheric circulation or cloud changes. In particular, it has been suggested that the enhanced evaporation from the ice-free ocean may lead to more persistent and denser clouds. Satellite retrievals suggest that in the autumn the Arctic stratus clouds have indeed become more dense and extensive over the last 10 years, or so (Palm et al., 2010). It is well known that in the Arctic the low clouds have a warming effect on the surface due to their enhancement of downwelling radiation (Intrieri et al., 2002). Therefore, one can envisage a positive feedback between shrinking sea ice (due to global warming), enhanced evaporation, increased effective cloud cover, enhanced downwelling longwave radiation and warming surface temperatures. However, such a feedback loop has not been established, and it can not be ruled out that the positive correlation observed over only a few years between sea ice extent and cloud amount may be a co-incidence. Furthermore, cloud properties may also change due to aerosol changes, e.g., due to increasing emissions of SO₂ from ship traffic, as well as di-methyl- sulfide (DMS), sea salt and primary organic matter from the open ocean. Such aerosol changes may render the clouds optically thicker (Lubin and Vogelmann, 2006), with a possible additional positive feedback loop.

Low clouds have a net warming effect in the Arctic [Intrieri *et al.* , 2002b],

as opposed to the well known net cooling effect they have at lower latitudes. Low layered clouds (stratus) also dominate the Arctic cloud cover. The Arctic climate changes have been greater than the global mean and have become known by the term "Arctic amplification" [Graversen *et al.*, 2008]. Therefore the climate effect of low clouds in the Arctic is an interesting topic to study.

Decreasing sea ice extent could lead to an increase in the aerosol number concentrations in the area where ice has retreated. The open sea surface it self would lead to an increase in release of sea salt and DMS (dimethyl sulfide) to the lower atmosphere. The lack of sea ice would also increase the likelihood that the sea could be used for shipping, which would pollute the area.

The enhancement of evaporation from diminishing sea ice and the increase in aerosol number concentration from open water and shipping could lead to denser and longer-lived low clouds in the area of sea ice retreat. A followup question to that is if these clouds would then have a slightly different radiative effect, and by that influence the further retreat of sea ice.

This warming is due the emission of longwave radiation that reaches the surface. At lower latitudes the clouds ability to reflect shortwave radiation would have a large enough cooling effect for the longwave emissions to be overpowered. In the Arctic the polar night in winter and high zenith angles in summer reduce the available shortwave radiation to reflect drastically, and the emission of longwave radiation outweighs the cooling effect by reflecting the shortwave radiation @*(cite Intrieri, the right one)*

1.1 Main goal

According to the IPCC report by Boucher *et al.* [2013] the study by Eastman & Warren [2010a] using visual cloud reports from the Arctic, with surface and satellite observations, and the studies by Kay & Gettelman [2009] and Palm *et al.* [2010] using lidar and radar observations have confirmed that the low-cloud amount over the Arctic oceans varies inversely with sea ice amount. This means that there is an increase in cloud amount when there is less sea ice. Now what we want to know is if these clouds are also denser and more persistent, and could lead to an enhanced warming and reduced sea ice amount, a positive feedback.

With this thesis I try to find if a decrease in Arctic sea ice lead to denser and more persistent clouds. It has been suggested that the decline in sea ice extent would allow for more pollution in the Arctic, as a consequence of more open water and ship traffic. The effect of increase in aerosol concentrations from shipping and open water, and the effect of enhanced evaporation from open water are studied separately and combined. With the main goal to find if this would lead to changes in clouds that could enhance downwelling

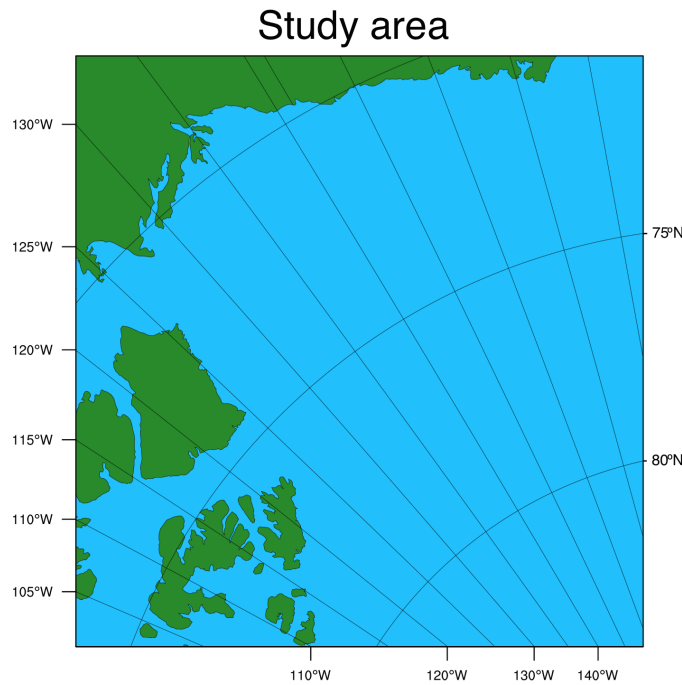


Figure 1.1: An overview of the study area. The bottom right corner is the northernmost point and the y-axes show longitude and latitude to the left and right, respectively.

long wave radiation and decrease upwelling short wave radiation, both of which have warming effects.

1.2 My contribution

The findings in my thesis have been achieved with some of the most recently developed code (by Greg Thompson [Thompson & Eidhammer, 2014]) for cloud micro physics and aerosols and their effects on radiation, in modeling. The results build further on the work of other researchers @name-some-and-cite and may raise some questions for further research within the field.

1.3 Area description

The area of the study in this thesis is in the Arctic, north of the United States of America and north-west of Canada. The study area covers the Beaufort Sea and small parts of Alaska and Canada, and can be seen in figure 1.1.

There are a few reasons for choosing this as the study area. First it is in the Arctic, and sea ice is present there in autumn, even in 2012 when there

was record low sea ice extent (@cite web NSIDC). Also it has been subject to field campaigns: Surface Heat Budget of the Arctic Ocean (SHEBA) [Uttal *et al.*, 2002], First International Satellite Cloud Climatology Project Regional Experiment Arctic cloud Experiment (FIRE ACE) [Curry *et al.*, 2000], Mixed-Phase Arctic Cloud Experiment (M-PACE) [Verlinde *et al.*, 2007] and more. Therefore there are many studies on Arctic clouds that include this study area and data from some of the mentioned field campaigns. This provides parts of the science basis for my study and selection of literature and studies for comparison and questions. Quite a few studies are based on satellite data analysis and some of them are presented in the next chapter as background and motivation for my thesis.

1.4 Background

In this chapter I shall present some recent literature on the subject, that forms a basis for the study presented in this thesis.

A study by Schweiger *et al.* [2008] investigated the connection between sea ice variability and cloud cover over over the Arctic seas during autumn. They analysed the ERA-40 re-analysis products and some satellite data sets. They found that that sea ice retreat was linked to a decrease in low-level (surface to \sim 1.9 km) cloud amount and an increase in mid-level (\sim 1.9 to 6.1 km) clouds. They state that the decrease in static stability and deepening of the atmospheric boundary layer, following ice retreat, contribute to the rise in cloud level.

The study by Vavrus *et al.* [2010] investigated the behaviour of clouds, during intervals of rapid sea ice loss in the Arctic in the 21st century. The study was done by use of the Community Climate System Model (CCSM3). Their results support that cloud changes appear to accelerate rapid loss of sea ice in autumn, and possibly in winter. They also conclude that "the trends in total cloudiness during rapid ice loss events are explained almost entirely by low-level clouds" and that "a positive feedback from primarily low cloud changes amid a warming climate".

Kay & Gettelman [2009] combined satellite data and complementary data sets to study the Arctic cloud and atmospheric structure during summer and early Autumn over the years 2006-2008. This covers the at the time record low sea ice extent from 2007. In contrast to the study by Schweiger *et al.* [2008] they found more low-level cloud. There are reasons to believe that the observations used in their study are more accurate than the re-analysis used in Schweiger *et al.* [2008].

Eastman & Warren [2010b] analysed visual cloud reports from the Arctic for year-to-year variations and found that following a low-ice September there would be enhanced low cloud cover.

The study by Palm *et al.* [2010] using satellite and lidar data and found

that areas of open water were associated with greater polar cloud fraction.

A common uncertainty and missing link in a few of these studies is that they did not look at liquid water content, effective radii and other parameters affecting the radiative properties of the clouds. In this study, that is what I want to look in to, how these properties are influenced by the changing sea ice, and if the clouds enhance the sea ice melt.

1.5 Structure of the thesis

In the following chapter, Chapter 2, the most important theory needed to understand some of the processes in clouds and their possible effect on the sea ice is presented. Chapter 3 is where I explain which model and tools and I have used and how I have worked with them to get the results presented and discussed in chapter 4. A summary of main findings and conclusions are presented in the last chapter 5.

Chapter 2

Theory of Clouds and Radiation

In this thesis the term shortwave (SW) refers to the wavelength band that carries most of the energy associated with solar radiation, including the visible spectrum and the shorter waves in the near infrared ($\lambda < 4\mu m$ [Wallace & Hobbs, 2006]). Longwave (LW) refers to wavelengths emitted by the earth-atmosphere system (terrestrial radiation) including the longer waves in the near infra red and wavelengths in the infrared spectrum ($\lambda > 4\mu m$ [Wallace & Hobbs, 2006]).

In this chapter how cloud properties can influence radiation is presented, followed by a section on cloud effects on aerosols. Lastly a brief overview of clouds in the Arctic, with focus on stratus, is presented.

2.1 Cloud effects on radiation

The cloud microphysical properties that determine the cloud radiative properties include: the amount of condensed water, the size and shape of the cloud particles, and if the particles are liquid or ice [Curry *et al.*, 1996].

2.1.1 The Cloud – a gray body

Stefan–Boltzmanns law states that the flux density emitted by a blackbody is proportional to the fourth power of the absolute temperature [Liou, 2002].

$$F = \epsilon_\lambda \sigma T^4 \quad (2.1)$$

where $\epsilon_\lambda = 1$ is the emissivity for a blackbody at wavelength λ . F ($W m^{-2}$) is the flux density emitted by the body, and $\sigma = 5.67 \cdot 10^{-8} J m^{-2} sec^{-1} K^{-4}$ is the Stefan–Boltzmann constant. A blackbody both absorbs and emits at maximum, and the ratio of absorption and emission to the maximum is given by the absorptivity, α_λ , and the emissivity, ϵ_λ , for wavelength λ . Kirchoff's

law states that the absorptivity and emissivity for a medium are equal for each wavelength in the longer wavelength spectra: $\alpha_\lambda = \epsilon_\lambda$ [Liou, 2002]. Kirchoff's law is only applicable for LW radiation at local thermodynamic equilibrium in the lower 60-70 km of the atmosphere. Since this study focuses on the lowest 2 km of the troposphere, the law is applicable.

A cloud can be defined as a gray body, which means that α_λ and ϵ_λ are not maximum, $\alpha_\lambda = \epsilon_\lambda < 1$ [Liou, 2002].

The cloud LW emissivity, ϵ , is a measure of the emittance of LW radiation by the cloud. From Stefan-Boltzmann's law, equation 2.1, the flux density emitted by a body depends on the body's temperature and its emissivity. The cloud longwave emissivity is given by Liou [1992]

$$\epsilon = 1 - \exp(-k_v^c \text{LWP}) \quad (2.2)$$

where k_v^c is the mass absorption coefficient of cloud particles, LWP is the liquid water path, which is the vertically integrated amount of water, and is further explained in section 2.1.5. Equation 2.1 shows that if one assumes constant cloud temperature, the flux density emitted by the cloud increases with increasing ϵ , which increases with increasing LWP. Name some typical values, and calculate F?@ Check also, values for $k_v c$!!@

2.1.2 Cloud optical depth

Cloud optical depth (or cloud optical thickness), τ , is a measure of the cumulative depletion that a beam of radiation directed straight downward (zenith angle $\theta = 0$) would experience in passing through a defined cloud layer. Of the incident SW radiation on a cloud with optical depth τ , a fraction $e^{-\tau}$ is not scattered and is defined as the transmissivity of the cloud – the radiation that is not absorbed or scattered in passing through the cloud [Wallace & Hobbs, 2006]. The remaining $1 - e^\tau$ has been scattered one or more times in passing through the cloud layer. The cloud optical depth is given by [Twomey, 1977]

$$\tau = \int_0^h k_E dz = \pi \int_0^h \int_0^\infty r^2 Q_E(r/\lambda) n(r, z) dr dz \quad (2.3)$$

at height z above cloud base for a cloud of depth h , containing $n(r)dr$ drops with radius in the interval $(r, r+dr)$ per cubic centimeter (cm^{-3}). $Q_E(r/\lambda)$ is the extinction efficiency and k_E is the extinction coefficient [Twomey, 1977]. The extinction efficiency is a measure of how well a particle removes the incident radiation, either by scattering or absorption. In the visible, for $\lambda \ll r$, $Q_E \approx 2$ is a good approximation [Hobbs, 1993], and we get the simpler expression

$$\tau = 2\pi N r_e^2 h \quad (2.4)$$

where it is assumed that the cloud droplet radius can be approximated by the effective radius, r_e .

2.1.3 Cloud albedo

In section 2.1.2 it was stated that the incident SW radiation on a cloud layer is either transmitted or scattered. The scattered radiation is scattered by single droplets, and the single-scattering albedo, $\bar{\omega}$, is the fraction of energy that is not absorbed in a single-scattering event, but scattered. $\bar{\omega}$ can to a good approximation be assumed equal to 1. Which means that the absorption of SW is negligible for cloud water, which supports that the SW radiation is either transmitted or scattered. When the single-scattering albedo is taken to unity, the albedo (or reflectance) of a cloud layer is given by [Hobbs, 1993]

$$A = \frac{(1-g)\tau}{1 + (1-g)\tau} = \frac{1-g}{\frac{1}{\tau} + (1-g)} \quad (2.5)$$

The cloud albedo, A , is then a function of the SW optical depth of a cloud, τ , and the asymmetry factor g . The asymmetry factor gives the direction of scattered radiation by the cloud, and is given by $g = \cos \theta$ where θ is the scattering angle. g is a power-averaged value of the cosine of the scattering angle [Twomey, 1974]. $g = 1$ indicates pure forward scattering and $g = -1$ indicates pure back-scattering. According to Twomey, $g = 0.8$ or 0.9 for warm clouds, which means that most of the scattered energy is scattered forward.

2.1.4 Cloud droplet effective radius

The cloud droplet effective radius determines important radiative properties of a cloud, cloud albedo (A) and cloud emissivity (ϵ) [Hansen & Travis, 1974], and is therefore of particular interest.

The cloud droplet effective radius is a mean of the size distribution of cloud droplets, weighted by the droplet cross section. The effective radius, r_e , may be written

$$r_e = \frac{\int r^3 n(r) dr}{\int r^2 n(r) dr} \quad (2.6)$$

It can be seen from equation 2.4 that a decrease in r_e , when N and h is kept constant decreases the optical depth of the cloud. Whereas an increase in r_e increases the cloud optical depth. It has already been established from equation 2.5 that a(n) decrease (increase) in the cloud optical depth leads to a(n) decrease (increase) in the cloud albedo A . The effect of r_e on ϵ is through the LWP and is described in the following section.

The effective radius is typically on the order of a few micro meters μm . Typical size of a cloud droplet is depicted in figure 2.1. The figure also

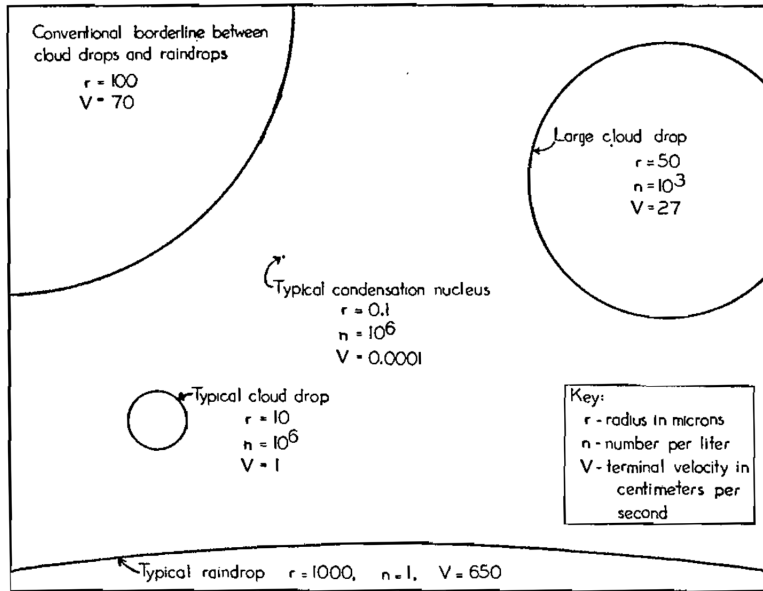


Figure 2.1: Typical sizes of cloud condensation nuclei (CCN), cloud droplet, large cloud droplet, borderline between cloud droplet and raindrop and typical size of raindrop. From [McDonald, 1958].

includes typical sizes of cloud condensation nuclei (CCN), large droplet, borderline between cloud droplet and raindrop and typical size of a raindrop.

2.1.5 Liquid water content and path

The amount of condensed water can be expressed by the liquid water content (LWC) in the cloud, often presented with units g m^{-3} and is proportional to the cloud droplet number concentration (CDNC), and cloud particle size. From Rogers & Yau [1989] the number of droplets with radius r can be expressed by

$$N = \int n(r)dr \quad (2.7)$$

where N is the CDNC (cm^{-3}), and $n(r)$ is the number of droplets with radius r . If the radius is approximated to be the mean volume radius \bar{r} , the

LWC for spherical droplets can be written

$$\text{LWC} = \int \rho_l \frac{4}{3} \pi r^3 n(r) dr \quad (2.8)$$

$$= \frac{4}{3} \pi \rho_l \int r^3 n(r) dr \quad (2.9)$$

$$= \frac{4}{3} \pi \rho_l \bar{r}^3 \int n(r) dr \quad (2.10)$$

$$= \frac{4}{3} \pi \rho_l \bar{r}^3 N \quad (2.11)$$

where the last equation shows the proportionality of LWC to the cloud droplet number concentration N , and to \bar{r} . ρ_L is the density of liquid water. Knowing the effective radius from equation 2.6, it is preferred to express the LWC as a function of that. The effective radius r_e and \bar{r} are related by

$$r_e = \kappa \bar{r} \quad (2.12)$$

where $\kappa = 1.14$ for continental clouds and $\kappa = 1.08$ for maritime clouds [Martin *et al.*, 1994]. κ is close to unity and if it is simply taken to unity the LWC may be written

$$\text{LWC} = \pi \rho_l r_e^3 N \quad (2.13)$$

Another common measure of condensed water is the liquid water path (LWP). If the LWC is integrated over a column, from the base to the top, it gives the LWP of that column.

$$\text{LWP} = \int_{base}^{top} \text{LWC} dz \quad (2.14)$$

The LWP is the column of liquid water in a cloud and is usually expressed in g m^{-2} .

What effect a change in LWP has on incoming and outgoing radiation can be seen when the cloud optical depth is expressed as a function of LWP. Recall the cloud optical depth for SW radiation from equation 2.4 and rewrite it to get the CDNC (N) on the left side

$$N = \frac{\tau}{2\pi r_e^2 h} \quad (2.15)$$

If the equation for LWC, equation 2.13, is also rewritten to get N on the left side, like so

$$N = \frac{3\text{LWC}}{4\pi \rho_l r_e^3} \quad (2.16)$$

the cloud optical depth in the visible (τ) can be written as a function of

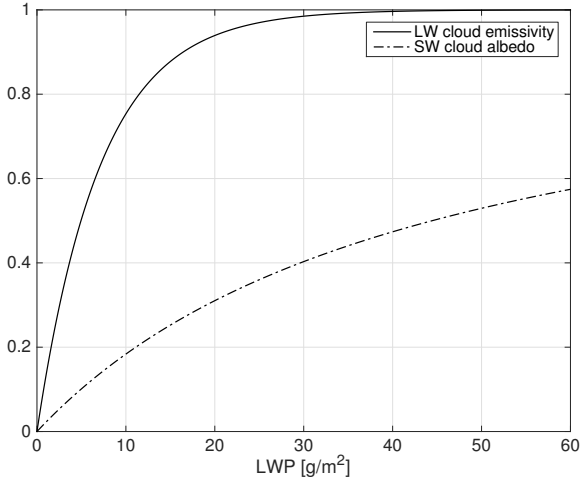


Figure 2.2: Cloud LW emissivity and SW albedo as a function of liquid water path (LWP), for clouds containing no ice.

LWP and r_e :

$$\frac{\tau}{2\pi r_e^2 h} = \frac{3\text{LWC}}{4\pi\rho_l r_e^3} \quad (2.17)$$

$$\tau = \frac{2\pi r_e^2 h 3\text{LWC}}{4\pi\rho_l r_e^3} \quad (2.18)$$

$$\tau = \frac{3\text{LWC}h}{2\rho_l r_e} \quad (2.19)$$

$$\tau = \frac{3\text{LWP}}{2\rho_l r_e} \quad (2.20)$$

Where LWC $h \approx$ LWP. It is now clear that, if the droplet size is constant, an increase in the LWP increases the optical depth of a cloud, τ . An increase in τ would make the denominator in equation 2.5 for the cloud albedo, A , smaller and thereby increase the cloud albedo. An increase in A also means a reduction in SW radiation reaching the surface. In that way, an increase in LWP would have a cooling effect on the surface. But, the LW radiation must also be considered. A change in LWP changes the cloud emissivity. Equation 2.2 shows that ϵ increases (decreases) with increasing (decreasing) LWP. Meaning that an increase in LWP would increase the flux density emitted by the cloud, following Stefan-Boltzmann's law from equation 2.1, and have a warming effect on the surface. Thus, a change in LWP gives opposite effects warming for shorter and longer wavelengths.

In figure 2.2 both SW cloud albedo, A , and the LW cloud emissivity, ϵ , are shown as functions of the LWP for ice-free clouds. It is based on equations 2.2, 2.5 and 2.20, where $k_v^c = 0.14$, $g = 0.85$, $\rho_l = 1000\text{kg/m}^3$ and

$r_e = 10\mu\text{m}$ which is a typical cloud droplet radius according to figure 2.1. A cloud emissivity less than unity is mainly a consequence of low LWP, as it is saturated in the LW already at a LWP of 40 to 45 g/m². A further increase in LWP does not increase the LW emission by the cloud and hence not the downward LW at the surface, but it does on the other hand still increase the cloud albedo. The increase in reflected SW radiation with LWP would thus work to even out the effect of emission of LW to the ground.

2.1.6 Ice water path

Clouds also consist of ice, not just liquid water. The amount of ice in a cloud for a given ice crystal size distribution is given by the ice water content (IWC) Liou [2002]

$$\text{IWC} = \int V \rho_i n(L) dL \quad (2.21)$$

where L is the maximum dimension of an ice crystal, V is the volume, ρ_i is the density of ice and $n(L)$ is the ice-crystal size distribution. As for the water droplets the cloud optical depth, τ , and mean effective crystal size, D_e , are related through

$$\tau \approx \text{IWP}(c + b/D_e) \quad (2.22)$$

where IWP denotes the ice water path $\text{IWP} = \text{IWC} \cdot h$ for a layer of thickness h , and $c \approx -6.656 \times 10^{-3}$ and $b \approx 3.686$ for ice columns [Liou, 2002]. Equation 2.22 clearly shows that an increase in the IWP increases the cloud optical depth (when D_e is kept constant), which in turn, according to equation 2.5, increases the cloud albedo. The opposite is obvious for D_e ; when D_e increases, the optical depth decreases, provided the IWP is unchanged, which in turn decreases A .

2.2 Aerosols and clouds

Aerosols have a direct effect on the climate by scattering and absorbing SW radiation, and scattering, absorbing and emitting LW radiation. A small subset of the atmospheric aerosols also serve as particles which water vapor can condense on to form droplets [Wallace & Hobbs, 2006]. Aerosols upon which water vapor can condense are called cloud condensation nuclei (CCN). Typical size for CCN is shown in figure 2.1. For low temperatures (~ -20 to -5°C) [Wallace & Hobbs, 2006], a few aerosols act as ice nuclei (IN) which if present allow for cloud ice to form. With IN cloud ice can form through heterogeneous freezing, contact nucleation and deposition [Wallace & Hobbs, 2006]. Heterogeneous freezing is when a droplet already contains a freezing nucleus and is brought to lower temperatures so that the already condensed

water on the particle freezes. Contact nucleation is when a supercooled droplet (droplet with temperature below 0°C) is hit by a suitable ice nucleus, and deposition is when water vapor freezes directly on the nucleus.

Some typical CCN are sulfates, sea salt and organic carbon, whereas IN are typically mineral dust, and are all included in the model used in this study [Thompson & Eidhammer, 2014], which is described in the next chapter. Typical aerosol number concentrations are 10^3 to 10^5 cm^{-3} , the number of those that can act as CCN range from 10^{-2} to 10^3 cm^{-3} , and the number of available IN is about 10^{-3} cm^{-3} . Through clouds these aerosols that act as CCN or IN also have an indirect effect. The amount of CCN and IN available affect the properties of the clouds. There are two known indirect effects that aerosols have on climate, through clouds.

2.2.1 The first indirect effect

The first indirect effect was proposed by Twomey [1974] and is often referred to as the Twomey effect. It describes the enhancement of cloud albedo as a consequence of an increase in aerosol content and thereby available CCN.

If there are few CCN in an area, a cloud formed there would be a clean cloud with few, but large droplets and therefore have a low albedo. If the area had high aerosol concentration, the cloud would be polluted and have more numerous but smaller droplets, provided the LWP is the same, which means it would have a higher optical depth in the SW according to equation 2.20, which through equation 2.5 gives a higher albedo.

The increase in cloud albedo due to pollution is shown in the left-most 4 figures in figure 2.3. The figure shows that with more CCN available, in a polluted environment, the cloud or cloud layer, appears brighter than when the air is clean (fewer available CCN).

Equation 2.4 shows that, if the effective radius is kept constant, the cloud optical depth will change with changes in CDNC (N in the equation). The CDNC is affected by the number of available CCN, and as the aerosol number concentration changes so will the number of CCN, and hence the CDNC and optical depth. Furthermore if a cloud has many small droplets, the cloud optical depth will be higher. Whereas fewer cloud droplets will yield a lower optical depth, provided r_e is kept constant, resulting in more SW radiation reaching the ground. The same is clear for ice, from equation 2.22, where it was shown that a larger ice crystal size yields a lower albedo, provided the IWP is unchanged. Thus the first indirect effect also applies to ice, since a decrease in D_e , while IWP is kept constant, means an increase in particle number, but a decrease in particle size and hence an increase in τ which in turn increases the cloud albedo.

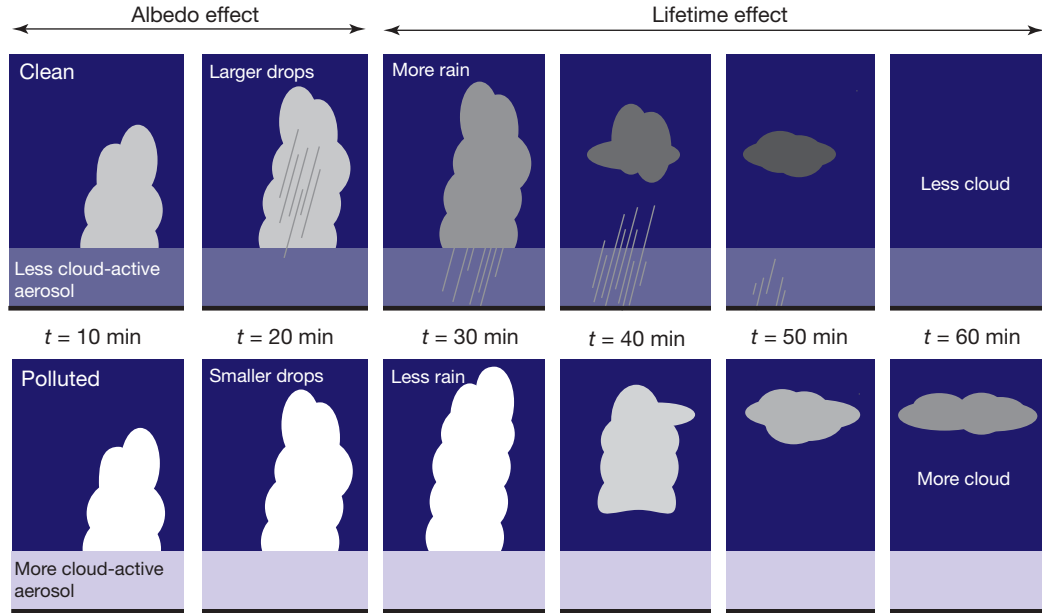


Figure 2.3: Figure showing the first indirect effect (albedo effect) to the left and the second indirect effect (lifetime effect) to the right. The figure includes a time axis to show the time scale of a precipitation process. The upper and lower panel show the clean and polluted case respectively. The figure is taken from Stevens & Feingold [2009].

2.2.2 The second indirect effect

The second indirect effect was proposed by Albrecht [1989], and is also known as the lifetime effect.

The second indirect effect suggests more numerous but smaller droplets reduce the precipitation efficiency and by that enhances the cloud lifetime and hence the cloud reflectivity [Albrecht, 1989]. The effect is depicted in figure 2.3 as the lifetime effect, where it is shown that in the lower panel, the polluted case, the cloud does not precipitate and is therefore still present after an hour, whereas the cloud in the upper panel, the clean case, is gone due to precipitation. If a cloud does not precipitate one could expect it to keep more of its liquid water for a longer time, by that increasing the lifetime of the cloud, and as shown by equation 2.20, a higher liquid water gives a higher optical depth and thereby also a higher albedo (equation 2.5).

Figure 2.1 shows that droplets have to grow to a size of typically $1000\mu\text{m}$ for precipitation to form. A rain drop is formed when smaller droplets collide and coalesce into a larger droplet, which also fails to collect smaller droplets until it is large enough to fall out of a cloud as precipitation. The second indirect effect suggests that an increase in aerosol burden leads to the water

vapor being spread over a higher number of droplets, giving them a smaller effective radius which will prohibit them from growing to a raindrop. The hypothesis is that if the cloud does not precipitate, it will grow denser and live longer since the cloud water is not removed by precipitation. According to Lohmann & Feichter [2005] this effect had been estimated to be of the same order as the first indirect effect. It has since been shown that the effect is in fact small globally averaged [Stevens & Feingold, 2009]. Stevens & Feingold [2009] state that in the cases where an increased aerosol burden prohibits precipitation, the cloud can be entrained by dryer air which leads to evaporation of the cloud droplets, and the cloud ceases to exist. On the other hand, an increase in aerosol burden in deep precipitating clouds may lead to more, not less precipitation [Stevens & Seifert, 2008].

2.3 Arctic clouds

Clouds in the Arctic differ from clouds elsewhere in that they have a net warming effect, as opposed to the global mean net cooling effect [Shupe & Intrieri, 2004]. Winter in the Arctic (polar night) is completely dark and free of incoming SW radiation. The Arctic summer on the other hand has sunlight 24/7. The amount of solar radiation reaching the surface is limited by the optical depth of the atmosphere it passes through. The normal optical depth is a measure of the cumulative depletion of a radiation beam directed straight downward (zenith angle $\theta = 0$) from the top of the atmosphere to a level z , defined by [Wallace & Hobbs, 2006]

$$\tau_{norm} = \int_z^\infty k_\lambda \rho_a R dz \quad (2.23)$$

where k_λ is the mass absorption coefficient, ρ_a is the density of air and R is the mass of absorbing gas per unit mass of air. The undepleted fraction of the radiation is given by the transmissivity, T_λ , of the layer. The transmissivity depends on the normal optical depth and the angle at which the beam deviates from straight down, the zenith angle θ . The transmissivity is defined by [Wallace & Hobbs, 2006]

$$T_\lambda = e^{-\tau_{norm} \sec \theta} \quad (2.24)$$

It is obvious that T_λ decreases with increasing θ . Since the Arctic is far North, the incoming solar radiation is at a high zenith angle, and less SW reaches the surface than at lower latitudes. Consequently the SW reaching the surface in the Arctic is low compared to lower latitudes. Low clouds have a net cooling effect globally, due to their high albedo. Clouds not only reflect SW radiation, but also emit LW radiation. When there is little SW to reflect, the warming effect of the emission of LW radiation is enhanced.

Clouds in the Arctic are mostly optically thin and low lying [Curry *et al.*, 1996].

The clouds studied in this thesis are low (up to about 1600 m) stratus clouds, in the Arctic. Stratus clouds are low layered clouds that form when extensive areas of stable air is lifted. They are normally between 0.5 and 1 km thick, and can be several km wide [Aguado & Burt, 2010]. The largest amounts of low stratus clouds in the Arctic are over the ocean [Klein & Hartmann, 1993]. According to Klein & Hartmann [1993] stratus in the Arctic basin peaks during summer at nearly 62%, while during the winter season the stratus only accounts for 18% of the cloud cover. This leads them to conclude that the seasonal cycle of stratus in the Arctic is driven by the temperature cycle, thereby moisture content in the atmosphere, rather than the static stability.

As mentioned in Chapter 1 there is no solar radiation to reflect during winter and the polar night in the Arctic, whereas in the summer the zenith angle is so high that even though there is sunlight 24 hours a day the cooling effect in summer does not average out the heating effect the clouds have in winter. A high zenith angle, means that the radiation has to travel through more atmosphere, which gives a higher optical depth and stronger depletion of the radiation beam. Consequently, the low clouds' ability to absorb and emit terrestrial radiation dominates over their reflective effect on the solar radiation.

The stratus clouds in the Arctic are typically thin (check with Curry@). The air in the Arctic is very stable in winter (polar night), and clean since there are not many sources for pollution. In Autumn the sea ice extent reaches a minimum after the summer melt and leaves open water to influence low clouds and their properties. Some of the cloud radiative properties are presented in the next section.

The tools and methods used to study Arctic clouds in this thesis are described in the following chapter.

Chapter 3

Model and methods

To test the thesis hypothesis, a formulation of the Weather Research and Forecasting (WRF) Model called the Advanced Research WRF (ARW) has been used. The model is described in the first part of this chapter. Then follows a description of the model setup and the different physics schemes that were chosen for this study, before a summary of the different runs that were performed. Ending the chapter are two short sections on the input data and processing of the model output.

3.1 Description of the WRF-ARW Modeling System

The version of the WRF-ARW modeling system used is 3.6.1, which was released in April 2014. The model is primarily developed at the National Centre for Atmospheric Research (NCAR) in Boulder, Colorado. The ARW model is the first fully compressible conservative form nonhydrostatic model designed for both research and operational numerical weather prediction (NWP) applications [Skamarock & Klemp, 2008].

As can be seen from figure 3.1 the WRF-ARW Modeling System consists of four major programs [Wang *et al.*, 2015]:

- The WRF Preprocessing System (WPS)
- WRF-Data Assimilation (WRF-DA)
- ARW solver
- Post-processing & Visualization tools

WPS is used primarily for real data simulations [Wang *et al.*, 2015], like the study presented in this thesis. A real-data simulation means that it has been initialized by observations and reanalysis, not artificial data. WPS' functions include defining simulation domains, interpolating terrestrial data

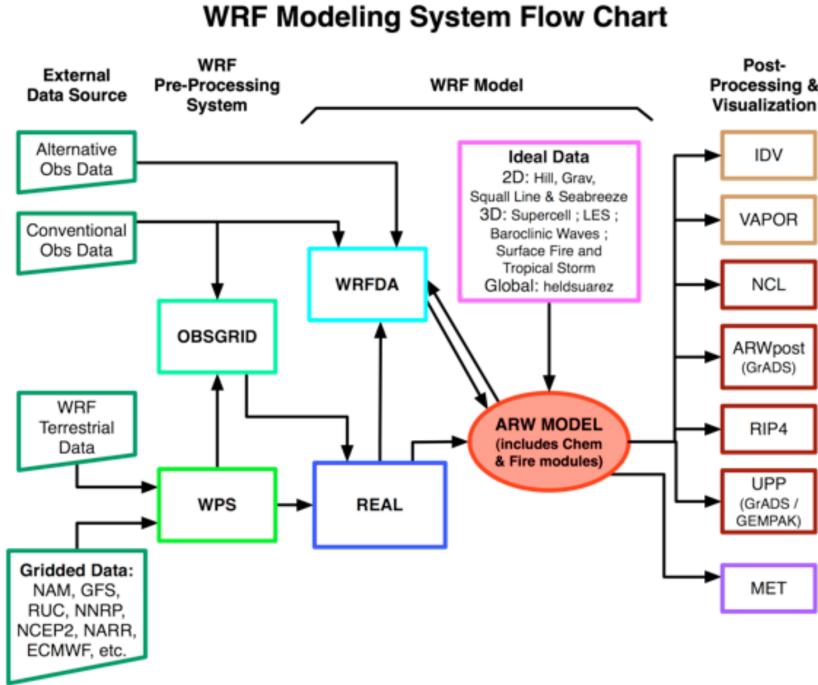


Figure 3.1: Flowchart for the WRF ARW Modeling System Version 3. From Wang *et al.* [2015].

and degridding and interpolating meteorological data from another model to this simulation domain [Wang *et al.*, 2015]. WRF-DA is optional and can be used to ingest observations into the interpolated analyses created by WPS [Wang *et al.*, 2015], but was not used in this study. The ARW solver is the key component of the modeling system, which is composed of several initialization programs for idealized, and real-data simulations, and the numerical integration program [Wang *et al.*, 2015].

The continuous equations solved in the ARW model are the Euler equations cast in a flux form where the vertical coordinate, η , is defined by a normalized hydrostatic pressure,

$$\eta = (p_h - p_{ht})/\mu \quad (3.1)$$

where $\mu = (p_{hs} - p_{ht})$ [Skamarock & Klemp, 2008]. p_h is the hydrostatic component of the pressure and p_{hs} and p_{ht} are the values of the hydrostatic pressure in a dry atmosphere at the surface and top boundaries respectively [Skamarock & Klemp, 2008].

The vertical coordinate is the traditional σ coordinate used in many hydrostatic atmospheric models, but is denoted by η in ARW, and is shown in figure 3.2.

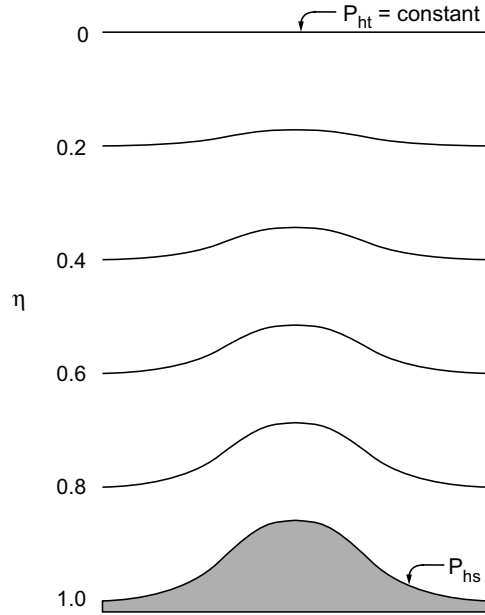


Figure 3.2: This figure is shown as presented in Skamarock & Klemp [2008], and is a schematic of the η coordinate. P_{hs} and P_{ht} represent the hydrostatic pressure at the surface and top respectively.

η decreases monotonically from a value of 1 at the surface, where the coordinate follows the terrain and $P_h = P_{hs}$, to a value of 0 at the top level, which is then a pressure surface, where $P_h = P_{ht}$. Levels with constant η are commonly referred to as η -levels (or Eta-levels). $\mu(x, y)$ is the mass of dry air per unit area within the column in the model domain at (x, y) . The η -levels are where the vertical wind speed is calculated, whereas the thermodynamic variables (θ) are calculated between the η -levels, on so-called mass levels.

With the vertical coordinate η , and the mass of an air column, $\mu(x, y)$, in the model grid the Euler equations can be written with variables on flux form:

$$\mathbf{V} = \mu \mathbf{v} = (U, V, W), \quad \Omega = \mu \dot{\eta}, \quad \Theta = \mu \theta$$

Now \mathbf{v} is the velocity vector in three dimensions, $\omega = \dot{\eta}$ denotes the vertical velocity and Ψ is the geopotential, and the set of prognostic equations that

needs to be solved numerically is this:

$$\partial_t U + (\nabla \cdot \mathbf{V}_u) - \partial_x(p\phi_\eta) + \partial_\eta(p\phi_x) = F_U \quad (3.2)$$

$$\partial_t V + (\nabla \cdot \mathbf{V}_v) - \partial_y(p\phi_\eta) + \partial_\eta(p\phi_y) = F_V \quad (3.3)$$

$$\partial_t W + (\nabla \cdot \mathbf{V}_w) + g(\partial_\eta p - \mu) = F_W \quad (3.4)$$

$$\partial_t \Theta + (\nabla \cdot \mathbf{V}\theta) = F_\Theta \quad (3.5)$$

$$\partial_t \mu + (\nabla \cdot \mathbf{V}) = 0 \quad (3.6)$$

$$\partial_t \phi + \mu^{-1}[(\mathbf{V} \cdot \nabla \phi - gW) = 0 \quad (3.7)$$

$$\partial_t Q_m + (\nabla \cdot \mathbf{V}Q_m) = F_{Q_m} \quad (3.8)$$

To close the system they use the diagnostic equation for inverse density, α_d ,

$$\partial_\eta \phi = -\alpha_d \mu \quad (3.9)$$

and the moist equation of state

$$p = p_0 \left(R_d \theta \frac{1 + R_d/R_v)q_v}{p_0 \alpha_d} \right)^\gamma \quad (3.10)$$

where $\gamma = c_v/c_p = 1.4$ is the ratio of the heat capacity for dry air at constant volume, to that of constant pressure, R_d and R_v are the gas constants for dry and moist air respectively, q_v is the mixing ratio of water vapor and p_0 is the reference pressure (typically 10³hPa). The right-hand-side terms in equations 3.3-3.6 and 3.8 represent forcing terms which arise from model physics, turbulent mixing, spherical projections, the earth's rotation, and moist physics [Skamarock *et al.*, 2008].

To solve these equations the WRF-ARW modeling system uses the spatial discretization known as a staggered C grid [Skamarock *et al.*, 2008]. Figure 3.3 shows the schematic of the grid and how the velocities, u and v , are calculated at the edges of each grid box both in the horizontal and in the vertical, half a grid box length away from the thermodynamic variable, which is calculated in the middle of each grid box, at the mass point. The advection in and out of the grid box is calculated from u and v . This staggering allows for discretization of the pressure gradient and divergence terms across a single grid interval, without any averaging, which gives a highly accurate second order difference.

The time integration in ARW is performed by a "time split integration scheme", which means that the low frequency, meteorologically significant modes are integrated by a third order Runge-Kutta (RK3) integration scheme, while the higher frequency acoustic modes are integrated with a shorter time step, to conserve the numerical stability. In general, it is preferred to use as large a time step as possible while keeping the numerical stability. For integration by the RK3 scheme the maximum time step Δt_{max}

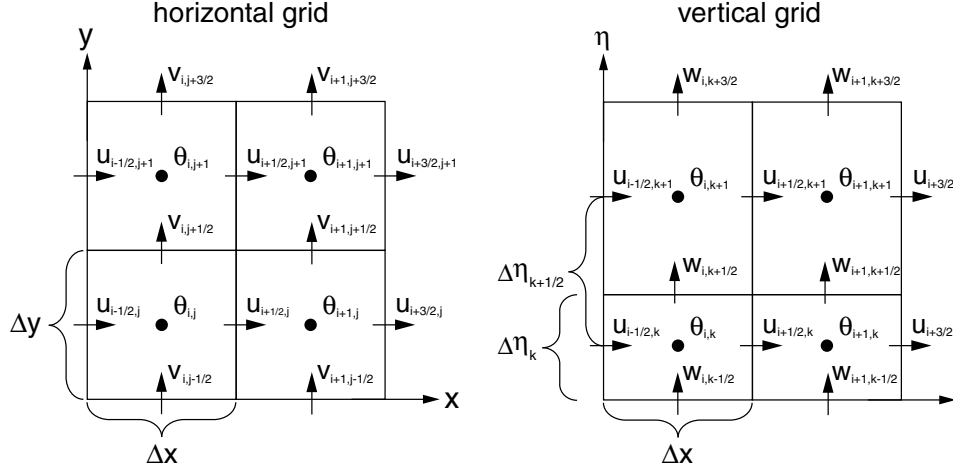


Figure 3.3: This figure is shown as presented in Skamarock & Klemp [2008], and shows the staggering of the C-grid. The horizontal staggering to the left, and the vertical staggering to the right.

is found through equation 3.11

$$\Delta t_{max} < \frac{C \cdot \Delta x}{\sqrt{3} \cdot u_{max}} \quad (3.11)$$

where C is the maximum Courant number, which depends on the order of the discretization of the advection terms. Typically in WRF, it is recommended that Δt (in seconds) does not exceed 6 times Δx (in km). When I ran the modeling system with a horizontal resolution of 4 km I therefore chose $\Delta t = 24$. More about the model runs and choices of physics in the model is presented in the next section.

3.2 Model setup

The model was ran with a $4 \text{ km} \times 4 \text{ km}$ horizontal grid point spacing, with 300×300 grid points, and 72 vertical layers, with the model top at 10 hPa. The area covers parts of the Beaufort Sea, by Canada and Alaska. This area was chosen because data from the area has been used for related studies [Intrieri *et al.*, 2002a, Kay & Gettelman, 2009, Palm *et al.*, 2010, Schweiger *et al.*, 2008, Shupe & Intrieri, 2004, Wu & Lee, 2012] as mentioned in Chapter 1. The area is not completely ice free any part of the year, and provides a good place to simulate cloud-sea ice interaction. The area is over several time zones but is approximately 7 hours behind UTC time. The times given in the WRF-ARW modeling system are UTC. The model was ran for a period of 5 days, 1st to 6th of September 2012. This is approximately when the record low ice extent in the Arctic was set (eg. National Snow and Ice

Data Centre, U.S.A., Beitler [2012]).

The vertical layers in the ARW model are often referred to as eta levels, because of the choice of η as the vertical coordinate. These levels have uneven vertical spacing and the altitude of each level is dependent on pressure, therefore the level height varies in both time and space. As a consequence of pressure dependence, the levels in the lower troposphere are closer to each other than the levels higher up in the troposphere. Thus the low clouds in the area can be resolved. Approximate heights for the lowest 11 eta levels are shown in Table 3.1.

Table 3.1: Approximate height for each level in meters above the surface.

Eta level	Approximate height
1	10 m
2	50 m
3	130 m
4	230 m
5	370 m
6	530 m
7	650 m
8	950 m
9	1250 m
10	1400 m
11	1600 m

3.2.1 Choices of physics in the model

The selection of physics schemes in WRF-ARW are numerous and fall into several categories, each containing several choices. Table 3.2 shows some of the different categories and the choice of scheme, for this study, within each of those categories.

Table 3.2: Table of physics categories and choice of scheme for this thesis

Physics categories	Scheme selected within category
(1) microphysics	aerorol-aware [Reisner <i>et al.</i> , 1998, Thompson & Eidhamer, 2014, Thompson <i>et al.</i> , 2004, 2008]. Option 28.
(2) cumulus parameterization	Grell 3D @cite authors. Option 5.
(3) planetary boundary layer (PBL)	Yonsei University scheme @cite authors. Option 1.
(4) land-surface model	Noah Land Surface Model @cite authors. Option 2.
(5) radiation	RRTMG LW & SW [Iacono, 2003, Iacono <i>et al.</i> , 2000, 2008, Mlawer <i>et al.</i> , 1997]. Radiation options 4.

The ARW model offers a wide selection of schemes to treat different physics that one wants represented in the model. The schemes treat the physics slightly differently and some schemes are better for certain horizontal and vertical resolutions than others, so one needs to be careful when choosing how the model is to treat the physics. For my thesis, the especially relevant scheme to mention is the cloud microphysics scheme that I chose, which is the aerosol-aware scheme described in Thompson & Eidhamer [2014]. When studying cloud and rediation response to removal of sea ice we might expect an increase in aerosols from the open ocean and increased sea traffic. The aerosols are therefore also relevant for the choice of schemes, and the aerosol-aware scheme includes the necessary processes for this study.

The choice of cumulus parameterization was based on the grid resolution, and the best fit for it. A horizontal grid point spacing of 4 km can be fine enough to not use cumulus parameterization [Thompson & Eidhamer, 2014], but in this thesis a parameterization that was more suitable for grid point spacings less than 10 km was chosen; the Grell 3D parameterization. According to Wang *et al.* [2015] Grell 3D may be used on high resolution, like my 4 km grid point spacing.

The aerosol-aware scheme

The microphysics includes explicitly resolved water vapor, cloud, and precipitation processes. The aerosol-aware scheme was chosen so that the study would have scavenging of aerosols included and have proper enough representation of aerosols to study aerosol-cloud interactions, without using the WRF model coupled with chemistry (WRF-Chem). According to the ARW User's Guide by Wang *et al.* [2015], the aerosol-aware scheme considers water- and ice-friendly aerosols, and a climatological dataset may be used

to specify initial and boundary conditions for the aerosol variables. I have used this climatological dataset, which is explained in Subsection 3.3.1 Input data. The scheme uses a monthly mean for aerosol number concentrations derived from multi-year (2001-2007) global model simulations in which particles and their precursors are emitted by natural and anthropogenic sources and are explicitly modeled with multiple size bins for multiple species of aerosols by the Goddard Chemistry Aerosol Radiation and Transport (GOCART) model [Thompson & Eidhammer, 2014]. The aerosol-aware scheme [Thompson & Eidhammer, 2014] is built on the schematic shown in figure 3.4, from Reisner *et al.* [1998]. It is a double moment scheme, which means it computes both mass mixing ratios, Q , and number concentrations, N , for the same water species (hydrometeors).

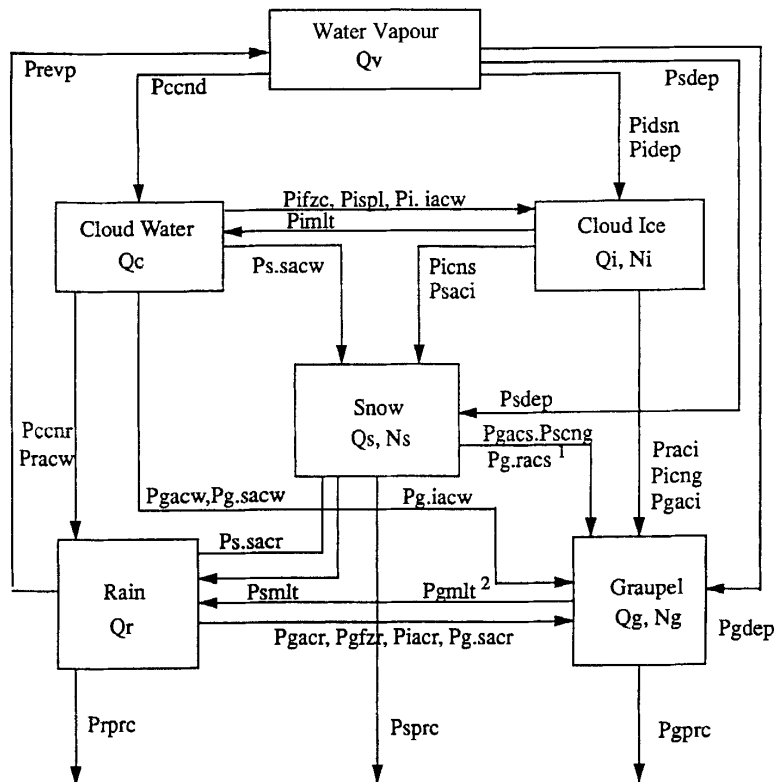


Figure 3.4: Cloud microphysical parameterization scheme used in some NWP models as shown in Reisner *et al.* [1998]. A full list of the acronyms used in the schematic can be found in Reisner *et al.* [1998].

Figure 3.4 show the processes in the microphysics scheme developed by Reisner *et al.* [1998], which the first bulk microphysics scheme by Thompson [Thompson *et al.* , 2004] was based on. The aerosol-aware scheme [Thompson & Eidhammer, 2014] is an extension of the updated Thompson bulk

microphysics scheme described in Thompson *et al.* [2008]. The figure shows a schematic of five hydrometeors, cloud water (c), rain (r), ice (i), snow (s) and graupel (g), and if just the mass mixing ratio is calculated or if both the mass mixing ratio and the number concentration is calculated. For each of the hydrometeors, prognostic equations are used with all the sources and sink terms included.

The RRTMG radiation schemes

According to Thompson & Eidhammer [2014] the Rapid Radiative Transfer Model (RRTM) for General Circulation Models (GCMs) (RRTMG) schemes for SW and LW [Iacono, 2003, Iacono *et al.*, 2000, 2008, Mlawer *et al.*, 1997] are the only radiation schemes which include the effects of the effective radii calculated in aerosol-aware. These were therefore used in combination with the aerosol-aware cloud microphysics scheme. The RRTMG schemes are accurate schemes using look-up tables for efficiency, and accounts for multiple bands and microphysics species, and includes the Monte Carlo Independent Column Approximation (MCICA) method of random cloud overlap [Wang *et al.*, 2015].

3.3 Model runs

The results presented in the next chapter are based on four different runs. The control run is the run where the aerosol climatological dataset has been used unchanged, and where the sea ice is kept as it was in the downloaded input data, see Subsection 3.3.1. The control run is used as a base to compare the other runs to, those with no ice and/or increased aerosol number concentrations.

There are three runs where the sea ice was removed, NoIce, Aero10NoIce and Aero100NoIce. The point of this is to compare the run with no ice to the control run, and see if there are any changes in the cloud properties, and SW and LW fluxes. For two of those runs the aerosol number concentration was also increased, these can be compared with the control run, and the other runs that have ice, but the same aerosol number concentrations.

The number of water- and ice-friendly aerosols were multiplied by 10 both with and without sea ice for 2 runs: Aero10 with ice, and as mentioned above, Aero10NoIce without ice. The goal is to find changes in cloud properties, and radiation fluxes compared to those in the control run.

Table 3.3 shows an overview of the different runs that have been executed, whose output have been used for production of figures presented in the next chapter.

Table 3.3: Table showing the names of the runs and if they have sea ice or not, and if the aerosol concentration has been increased by a factor of 10 through input files. All the runs have the same horizontal resolution of 4 km×4 km, dimensions 300×300, 72 vertical layers and $\delta t=24$ s.

Name	Sea ice	Aerosol concentration
control	initial	climatology
NoIce	removed	climatology
Aero10	initial	climatology×10
Aero10NoIce	removed	climatology×10

3.3.1 Input data

The model runs were initialized with data downloaded from the European Centre for Medium-Range Weather Forecasts (ECMWF). The downloaded data is from the ERA-Interim dataset, which is a global atmospheric reanalysis from 1979 to present and continues to be updated in real time. Through WPS the data from ERA-Interim was interpolated over the area, with a 2 degree minute spacing between the points, to be used to initialize the model. The data used is in 6-hourly atmospheric fields on pressure levels, for the first five days of September 2012, which was the period the model was run for. This is done to make sure the initial meteorological conditions are the same in every run, so that the effects of changing a variable in the input files for the modeling system are only due to that change.

To use the climatological aerosol dataset, the file containing monthly means had to be called through WPS. The aerosol input data includes mass mixing ratios of sulfates, sea salts, organic carbon, dust, and black carbon from a 7-yr simulation with 0.5° longitude by 1.25° latitude spacing [Thompson & Eidhammer, 2014].

3.3.2 Manipulation of input files

The input files for the ARW solver, created by WPS and REAL (see figure 3.1) were manipulated by use of the NetCDF Operator (NCO) tool ncap2. In these files the sea ice was removed for the runs without sea ice (NoIce and Aero10NoIce) and the aerosol number concentration from the climatological dataset was multiplied by 10 for the runs with increased aerosol concentrations (Aero10 and Aero10NoIce).

3.4 Processing of the results

Figures presented in my thesis, I made (unless other is stated) by use of NCL (National Centre for Atmospheric Research (NCAR) Command Language)

and/or MatLab. For the NCL scripts I found a lot of help and inspiration from the example scripts for WRF-users available at ([URL for examples](#)).

Chapter 4

Results and discussion

In this chapter, the findings made in the thesis are presented. This chapter mostly consists of a discussion of why there is a difference in certain cloud and radiation variables between the run with removed sea ice and the control run, and the run with increased aerosol number concentration and the control run. At the end, there is also a small section on the difference from the control run when both the sea ice is removed and the aerosol number concentration is increased.

The results are discussed separately for removed sea ice and increased aerosol number concentration and for days 1 and 5. Where day 1 represents the closest to an "off line" run, whereas by day 5 the atmosphere has had some time to adjust to the changes.

I also try to answer if these results show a warming or cooling effect and if there is reason to believe that changes in sea ice extent and aerosol concentration will further influence the sea ice extent.

The discussion is based on differences in daily averages for the fields. The daily averaged differences have been calculated by subtracting the field from the control run for one time from the same field at the same time from a different run, these differences have then been added together and divided by the number of differences that were added together.(@clarify!)

But first, to have a reference for the differences, the weather and cloud situation for the control run is presented.

4.1 The control run

Figure 4.1 shows the weather situation in the control run for days 1 and 5. The temperature at 2 m height is represented by red contour lines, and the wind speed and direction at 10 m height is shown by the wind barbs and their color. Day 1, figure 4.1a shows weak northerly winds ($\sim 5 \text{ m/s}$) bringing cold air, -3°C (270 K), from the north over the sea ice, and the westerly winds over the ocean south of the sea ice bring moisture to the

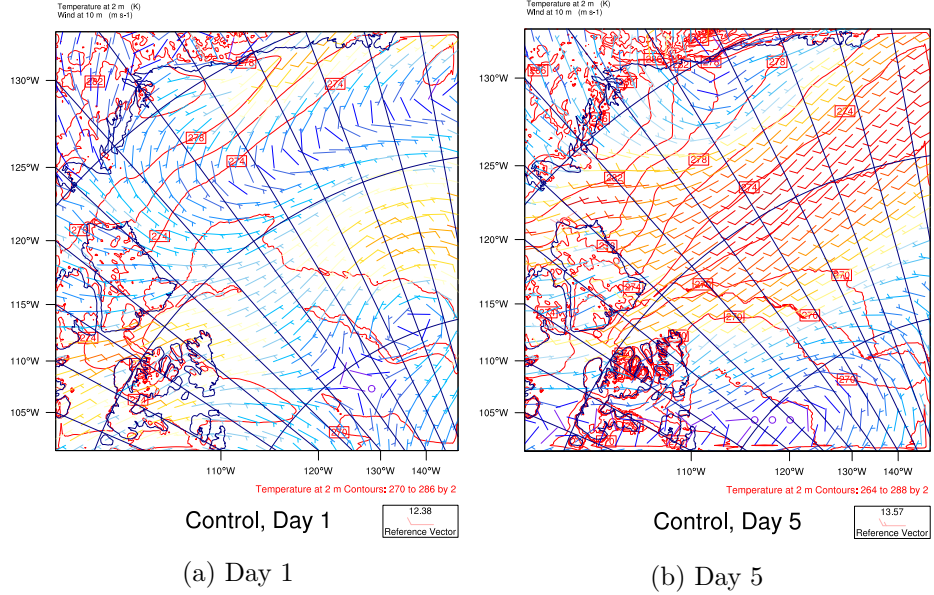


Figure 4.1: The temperature and wind pattern for days 1 and 5, from the control run. The temperature at 2 m height is represented by red contour lines and the wind speed and direction at 10 m height is shown by wind barbs and their color, where red is higher wind speed and blue is lower. The shortest tails on the wind barbs indicate a wind speed of 5 m/s and the longest indicate 10 m/s.

air over the sea ice which is contributes to the low stratus in figure 4.2a. Figure 4.2 contains the vertical cross sections of LWC and IWC over the line shown in figure 4.2d. The deeper clouds over the island in figure 4.2a have been formed due to orographic lifting, and the height of the "mountain" is ~ 400 m according to the y-axis in the cross section, and the filled contours of terrain height in figure 4.2d. The westerly winds over the sea ice, towards the mountain at $\sim 76^\circ\text{N}$ and 112°W , increase in strength of the mountain and brings air to saturation as it is lifted and forms deeper clouds over the mountain with LWC of $\sim 0.1\text{g/m}^3$. From figure 4.2b, showing the ice water content (IWC) in the section one can see that the thicker clouds over the mountain also contain ice in the upper part of the clouds, with about $5 \cdot 10^{-3}\text{ mg/m}^3$.

By day 5 the wind direction has changed to south-easterly, see figure 4.1b, and the clouds in the cross section, figure 4.2c are low stratus over the sea ice, and there is also some thin cloud formation at the mountain, probably formed by weaker orographic lifting. There is no IWC in the section for day 5 (not shown).

The LWP for days 1 and 5 are shown in figure 4.5a and 4.5b with the CDNC (4.3a and 4.3b) and r_e (4.6a and 4.6b). One can clearly see that

where the LWP is high, so is the CDNC, which is expected based on equation 2.13. The pattern in r_e is @different due to...@

The fluxes of both SW and LW radiation at both the surface and at the top of the atmosphere (TOA) may be partly explained by the clouds, through looking at the LWP. Figure (@radiation) shows the downward SW at the surface (@subfig) and upward at TOA (@subfig) for day 1 and @more radiation and why it looks that way.

The heat fluxes upward at the surface, latent heat (LH) and sensible heat (SH), are also of interest when studying clouds in the Arctic. The fluxes are shown in figure (@figure) for day 1 (LH (@subfig), SH (@subfig)) and day 5 (LH (@subfig), SH (@subfig)). Notice that the LH and SH is lower over the sea ice for both days 1 and 5. This because the sea ice is colder than the ocean, and works as a lid over that part of the ocean, not letting all the heat out.

4.2 Removed sea ice

The sea ice that was there in the control run, but has been removed for NoIce, is shown in figure 4.7.

4.2.1 Day 1

The average difference in LWP for NoIce - Control for day 1, shown in figure 4.8a, is slight for the shore field ($\sim 0.23\text{g/m}^{-2}$ increase). But the area of interest in this case is where the sea ice is not present, which it was in the control run (figure 4.7). The sea ice edge is also included as a black contour in figure 4.2d. The area where there was sea ice in the control run shows a positive difference in LWP. Especially furthest north (bottom right corner of the map) the LWP is significantly higher, $> 15\text{g/m}^2$.

This implies that there is a new cloud forming in that area, that could not form when there was sea ice. The removal of the sea ice has allowed for increased evaporation and an increase in latent heat (LH) flux which can be seen from figure 4.9a, where the shape of the area that sea ice was removed from is recognized. Figure

The northernmost part of the study area also has an increase in the cloud droplet number concentration (CDNC), figure 4.8b, in the same area as is covered by the red patch indicating an increase in the LWP, which fits well with equation 2.13, which was presented in chapter 2. There the amount of liquid water is proportional to the droplet number concentration, denoted by N in the equation, and the LWP is the vertically integrated LWC. The average increase in the CDNC would be approximately 1 or 2 droplets per cubic centimeter in the northernmost area. The figure shows the numbers with units $10^6/\text{kg}$, which can be approximated to the more common units for CDNC, per cubic centimeter (cm^{-3}). Assuming that the cloud is close

enough to the surface to assume a pressure $p = 1000\text{hPa}$, and thereby the density to be $\rho_a = 1\text{kg/m}^3 = 1\text{kg}/10^6\text{cm}^3$, then CDNC : $10^6/\text{kg} = \text{cm}^{-3}$. Since this is the average over 24 hours and 11 layers, to a height of about 1600 m, the CDNC could be higher at certain times, and in certain layers.

The increase in effective radius in the same area as the LWP is increased also indicates the formation of a new cloud, figure 4.8c, that could not form in the control run (see figure 4.6a).

The two red patches at 80°N and $140\text{-}155^\circ\text{W}$ in the figure for difference in r_e , figure 4.8c, is also clear in the difference in LW downward radiation, figure 4.10c at the ground surface, and can also be slightly recognized as a decrease in SW downward radiation, figure 4.10a. The SW radiation flux at ground surface has been reduced due to the increase in LWP, and the more pronounced decrease in SW is clearly recognized with the same shape and size as the northern patch of increase in LWP. This can be explained by equations 2.5 and 2.20, where it is clear from equation 2.20 that the cloud optical depth, τ , increases with LWP, and following equation 2.5 an increase in τ would also increase the cloud albedo.

The downward LW radiation flux at the surface has been increased due to the increase in LWP, which means that there is more water in the clouds and they emit more LW to the ground. It was shown in Chapter 2 that an increase in LWP increases the emissivity of the cloud, shown in equation 2.2, until the cloud is saturated with respect to LW radiation at about $40\text{-}45\text{g/m}^2$, following figure 2.2. The slight increase in the LW at TOA is because of increased temperature at the surface when the sea ice is removed (figure ??).

Of course, the removal of sea ice would reduce the SW at TOA, see figure 4.10b. The albedo of sea ice varies between 0.5 and 0.9 depending on snow cover and the age of the ice and is typically 0.5-0.7 for bare ice, whereas a typical ocean albedo is 0.06 [NSIDC, 2015]. Thus the change in SW at TOA is negative over the area of ocean where there was sea ice in the control run. The increased SW at TOA at 80°N and 155°W is because of the cloud forming in that area, see figure 4.10b, and can be recognized in the increase in r_e in the same place (figure 4.8c) which also represent an increase in LWP and reduction in SW at surface and increase of LW at surface. This is due to the enhanced albedo caused by new clouds at that location, since these figures don't show in-cloud changes, simply the difference between the fields from the run without ice and the control run.

The heat fluxes are almost unchanged for most of the study area by the removal of sea ice, except for the area where the sea ice has been removed (see figures 4.9a and 4.9b). Especially for the northernmost part of the study area and "sea ice removed area" the fluxes are a lot higher than in the control run. This is not surprising, since one would expect the ocean surface to hold a higher temperature than the sea ice. Also a lot more heat would be released due to evaporation than in the case when sea ice is present.

4.2.2 Day 5

The average differences for LWP, CDNC and r_e at day 5 are all negative, see figure 4.11, over the area that had ice in the control run. Thus the clouds making up the LWP in the control run, see figure 4.5b, have either ceased to exist, been significantly thinned, moved away or turned into ice. The LWP has a negative difference of $>30 \text{ g/m}^2$, which means that the LWP, when comparing with the values for that area in the control run (figure 4.5b) which were around $40\text{-}100 \text{ g/m}^2$, there is still around $20\text{-}70 \text{ g/m}^2$ left. So the clouds have not all ceased to exist. This is supported by the fact that the CDNC in the control run was ~ 10 to 25 cm^{-3} and has according to figure 4.11b got 3 to $>5 \text{ droplets cm}^{-3}$ less in the run with no ice. Then the clouds in the run with no ice are left with <5 to around $20 \text{ droplets cm}^{-3}$ which is definitely enough to assume that there are still clouds in the area.

There is hardly any ice at all in the study area in the lowermost 11 layers, much like in the control run (see figure 4.4b), and the IWP is zero (not shown) over the area where there was sea ice, and the area around. The wind pattern (not shown) is very much the same as in the control run (figure 4.1b), and the chance that the clouds have been moved to a different area is ruled out. Therefore precipitation must have depleted the clouds of some of droplets. The difference in rain (not shown) for the run with no ice compared to the control run is negligible and so snow was found guilty of depleting the clouds. Figure 4.12 shows how the cloud that was claimed started to form in day 1 of the run with no ice, in section 4.2.1, as more water vapor and aerosols were made available, develops into a snowing cloud and performs natural cloud seeding by snowing out the other clouds as it travels south-east over the sea ice free area.

Figure 4.12a shows the difference in mixing ratio of snow to air averaged for day 1 over the 11 lowermost layers. The slight increase in mixing ratio of snow is in the same area as the red patch in figure 4.11b that was claimed to be a forming cloud. Figure 4.12b shows that in day 2 the cloud has indeed formed and it starts its journey south-eastward and continues through to day 5, see figure 4.12e where the positive difference in snow is less pronounced, but still present.

The clouds in on the 5th day of the run with no ice is now significantly thinner than the clouds in the 5th day of the control run, due to the aforementioned reduction in CDNC. This allows for more of the upwelling LW at TOA to come directly from the surface, which holds a higher temperature than the atmosphere above (see cross section in figure 4.2c) and the newly ice free area also has a higher skin temperature, an increase of $\sim 1^\circ\text{C}$ than the area did in the control run, when there was sea ice there (see figure 4.14c). Following Stefan-Boltzmann's law (equation 2.1) the surface should now emit more LW than the clouds and sea ice with lower temperatures in the control run did. Figure 4.13d shows that the upwelling LW at

TOA has indeed increased by ~ 0.5 to 5 W/m^2 over the area where sea ice has been removed. Overall the average increase in upwelling LW at TOA for the whole area is just shy of 0.5, but the area of particular interest is where the sea ice has been removed, and that shows a more pronounced difference than the rest of the field.

In figure 4.13 the difference, for NoIce-Control, in SW down at the surface and up at TOA is illustrated by figures 4.13a and 4.13b. The upwelling SW at TOA (figure 4.13b) has an average difference of $\sim -3.3 \text{ W/m}^2$ for the whole field, and from <-25 to around -10 W/m^2 over the now ice free area. Such a decrease in upwelling SW radiation over the whole area that was covered by sea ice in the control run is because of the significant decrease in albedo of the area (not shown), which was discussed under day 1. The most pronounced decrease in upwelling SW at TOA at 77°N and 125°W is of same size and shape as the equally pronounced increase in downwelling SW at the surface of $>25 \text{ W/m}^2$ (figure 4.13a), in the same place. This can also be recognized as the most significant decrease in CDNC which has lost more than $5 \text{ droplets cm}^{-3}$ (figure 4.11b) compared to the control run. Thus, a cloud that was there in the control run has been significantly thinned or ceased to exist completely, such a decrease in CDNC (N in equation 2.4) decreases the cloud optical depth, τ , and albedo, A (equation 2.5), and does therefore not protect the surface from downwelling SW by reflecting it back to TOA.

The red patch at 77°N stretching from 120 to 140°W , in figure 4.13a, indicating the increase in downwelling SW is recognized as a decrease in downwelling LW in the same area in figure 4.13c. This can also be explained by the decrease in CDNC, or rather the LWP, where if the clouds are thinned or cease to exist, the LW emissivity of the clouds would decrease as the LWP decreased (equation 2.2), provided the LWP got lower than $40\text{-}45 \text{ g/m}^2$ according to figure 2.2. Looking at the difference in LWP in figure 4.11a, which shows LWP for NoIce-Control, one sees that the LWP in NoIce is $>30 \text{ g/m}^2$ less than in the control run for that exact area. The LWP in the control run (figure 4.5b) for that area was 30 to 60 g/m^2 . Thus the LWP in NoIce is below the limit for saturation on LW and the LW emissivity is decreased, explaining the decrease in LW reaching the surface in that particular area.

For quite a large part of the area which is now sea ice free the downwelling LW experiences an increase compared to the control run, difference shown in figure 4.13c. The depletion of clouds by snow, decreasing the LWP, would intuitively also decrease the downwelling LW at the surface if one considers the decrease in emissivity it would lead to, based on equation 2.2. On the other hand, knowing Stefan-Boltzmann's law (equation 2.1) the temperature of the emitting body is of crucial importance. The removal of sea ice has lead to an increase in surface heat fluxes and skin temperature, as mentioned in day 1, and shows the same for day 5 in figure 4.14.

A higher skin temperature and increased surface heat fluxes pushes the lower cloud limit slightly higher up into the atmosphere, the cloud height for a section of the area can be seen in the vertical cross section for LWC on day 5 4.15 for the run with no ice. Comparing this with the vertical cross section from the control run, figure 4.2c, it is clear that the stratus clouds lie approximately 500 m higher closer to the mountain in the NoIce run than they did in the control run.

Looking at vertical cross sections from NoIce and Control the clouds seem to have the same temperature in both runs, but in NoIce the cloud does not stretch as close to the mountain as in Control, and between 100 and 120 on the x-axis NoIce has no cloud, which fits with the decrease in downwelling LW in that area (77°N and 117°W). The increase in downwelling LW on the other hand might be explained by the increase in cloud height.men den forklaringen er jeg veldig usikker på

4.3 Increased aerosol concentration

4.3.1 Day 1

With an aerosol number concentration 10 times higher than that in the control run, the LWP and CDNC increase by about 11 g/m^2 and 16 cm^{-3} respectively, see figure 4.16. The increases in CDNC and LWP are expected with such a high increase in available CCN. Remembering the first indirect effect described in Chapter 2, one would expect a decrease in droplet size with the increase in numbers. r_e has in fact decreased for the whole field in this run, and is shown in figure 4.16c

The first indirect effect describes an increase in the cloud albedo as a consequence of more numerous and smaller droplets, and the upwelling SW at TOA is in fact increased by as much as $\sim 7 \text{ W/m}^2$ on average for the whole field on day 1 (see figure 4.17b). As opposed to the run with no ice, the sea ice is unchanged in the run with increased aerosol number concentration (Aero10), so the signal here is clearly an increase in reflected SW. Over the sea ice however the increase in reflected SW is not as large as in the rest of the field, since the sea ice already has a relatively high albedo itself (around 0.6). The increase in the albedo of the clouds have significantly reduced the downwelling SW at the surface (figure 4.17a) compared to the control run. The change is $\sim 9 \text{ W/m}^2$ decrease on average for the study area, which represents a cooling. On the other hand the average LW radiation at the surface is higher (figure 4.17c) due to the aforementioned increase in LWP and thereby increased emittance by the clouds, as follows from equation 2.2. The increase in LW reaching the surface is $\sim 2.3 \text{ W/m}^2$. The most pronounced increase in LW at the surface is in areas where the LWP in the control run (figure 4.5a) was lower and therefore not as close to saturation with respect to cloud LW emissivity. Two of these areas are

79°N, 135-140°W and 82°N, 125-135°W.

There is no clear response in the surface heat fluxes to the increased aerosol number concentration(not shown).

4.3.2 Day 5

The LW cloud emissivity is sensitive to an increase in water amount as long as the LWP is less than $\approx 40\text{-}45 \text{ g/m}^2$. Day 5 in the control run had LWP around 60-100 g/m^2 in the middle lower area of figure 4.5b. This is also seen in that there is no significant change in LW downward at the surface or upward at the TOA, see figures 4.19c and ??.

The area with lack of change in LW up or down is approximately the same area as where there is a negative change in LH and SH upward from the surface over the sea ice, see figure ???. Since there has been no change in LW there is no loss of warming from a decrease in LW reaching the surface, but the change can be explained by looking at the SW radiation. The downward SW at the surface has been significantly decreased as a consequence of the increase in aerosol number concentration, see figure 4.19a. Which is known as the first indirect effect, and was described in Chapter 2. The albedo of the sea ice in Aero10 is around 0.6 (not shown) which means that a fraction of the incident SW radiation is absorbed. Since the amount of incident SW radiation at the surface has been reduced by the cloud cover, the absorbed radiation is less than for a higher incident amount. The ice therefore has a lower temperature to give off SH with.

The skin temperature, figure ??, for the domain shows a small decrease in the same area as where there is less sensible and latent heat release.

Also the dynamics over ice and the ocean are different, so this could have an effect. The cold air over the ice may be intensified, while the sea surface temperature (SST) is the same for all the runs and there is no coupling with the ocean. There will therefore be no changes in the SSTs that could have an effect on the dynamics over the ocean. So the response may be smaller there...?

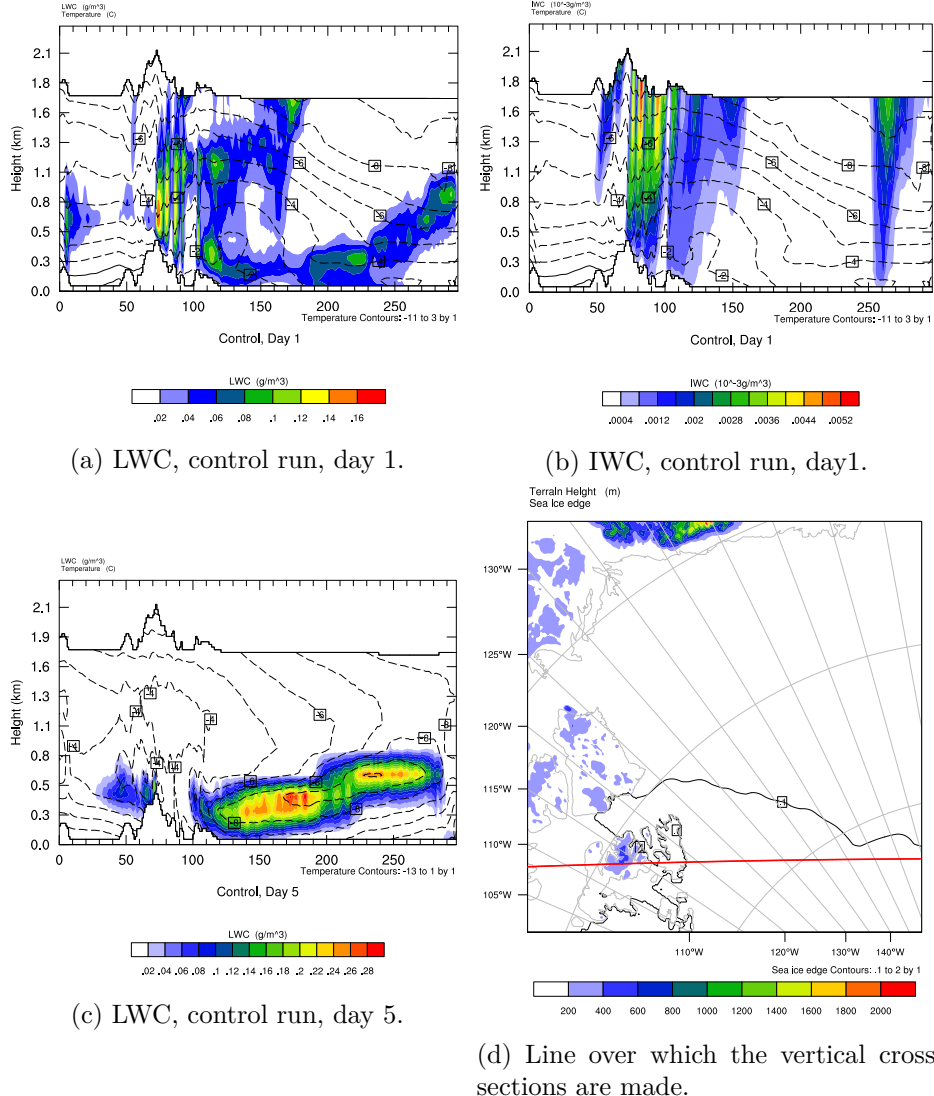
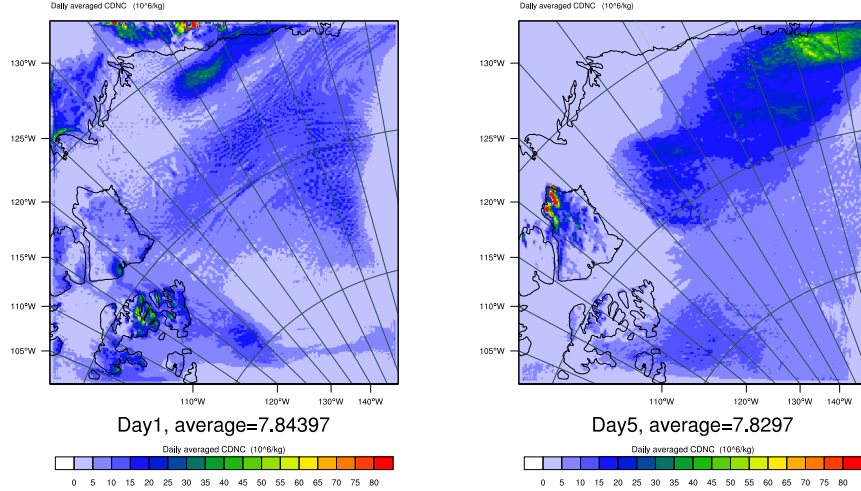
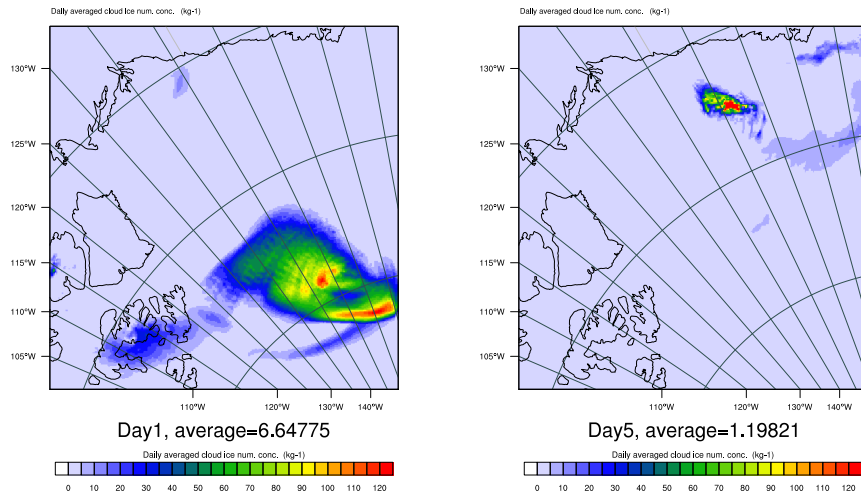


Figure 4.2: Vertical cross sections of averaged liquid (g/m^3) and ice (mg/m^3) water content, and temperature ($^\circ\text{C}$), from the control run, for days 1 and 5. LWC and IWC for day 1 are shown in figures 4.2a and 4.2b respectively. Figure 4.2c shows the LWC for day 5. The IWC on day 5 was 0 in the section and is not shown. Figure 4.2d shows a map of the area with the ice edge as a black contour line. The terrain height is represented by filled contours and the red line over the sea ice is the line over which the cross sections are made.



(a) Cloud droplet number concentration, averaged over the lower 11 layers and the 1st day.
(b) Cloud droplet number concentration, averaged over the lower 11 layers and the 5th day.

Figure 4.3: CDNC



(a) Cloud ice number concentration, plotted over the area, averaged over the lower 11 layers on the 1st day.
(b) Cloud ice number concentration, plotted over the area, averaged over the lower 11 layers on the 5th day.

Figure 4.4: CINC

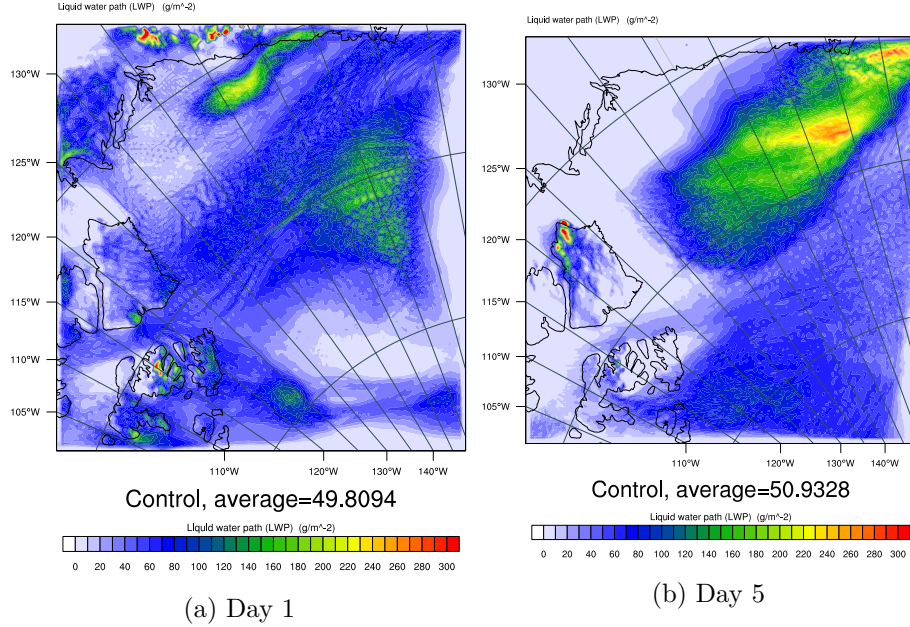
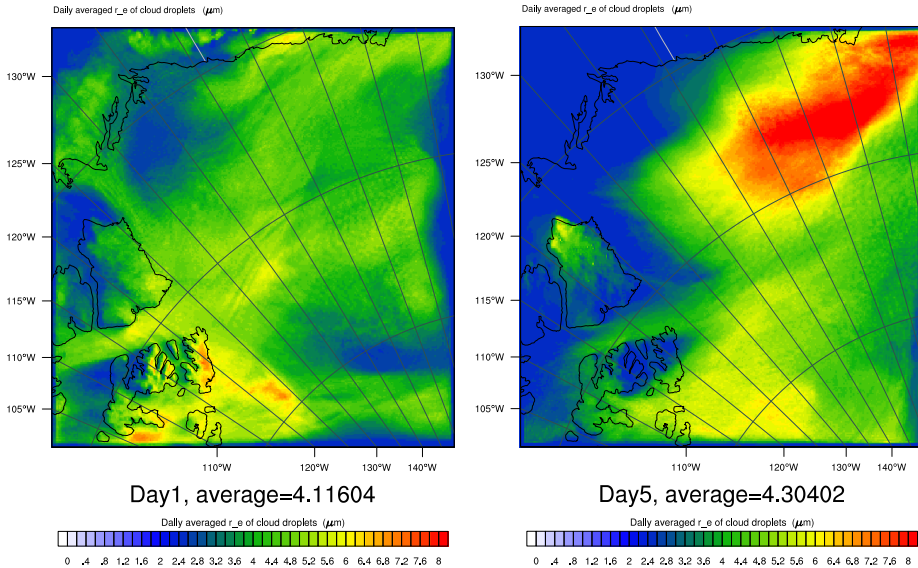


Figure 4.5: The average liquid water path (LWP) for days 1 and 5, including the average value for the field.



(a) The effective radius of cloud droplets average field for day 1 over the lower-most 11 layers. (b) The effective radius of cloud droplets average field for day 5 over the lower-most 11 layers.

Figure 4.6: Effective radius of cloud droplets (μm), averaged over the lowermost 11 layers for day 1 and 5.

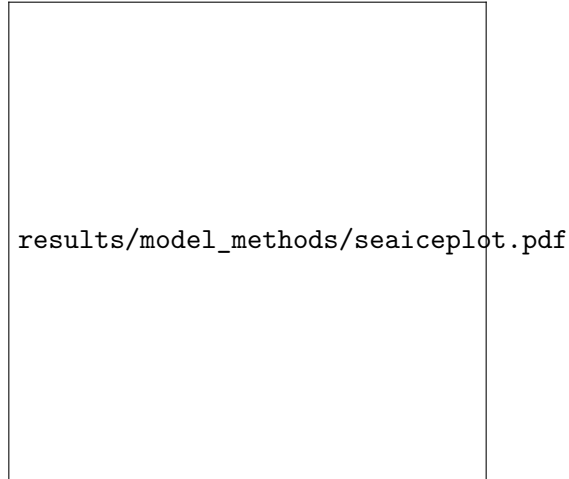


Figure 4.7: Sea ice fraction in Control (and Aero10).

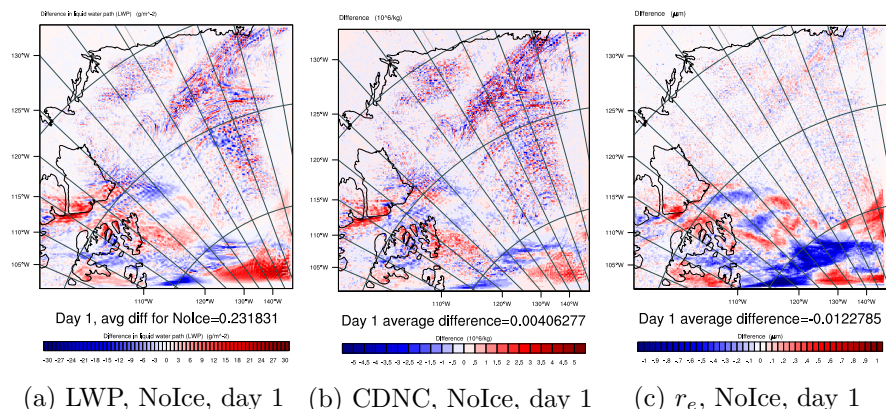


Figure 4.8: The averaged difference in LWP, CDNC and r_e of cloud droplets (from left to right) over the lowermost 11 layers for day 1. NoIce-Control.

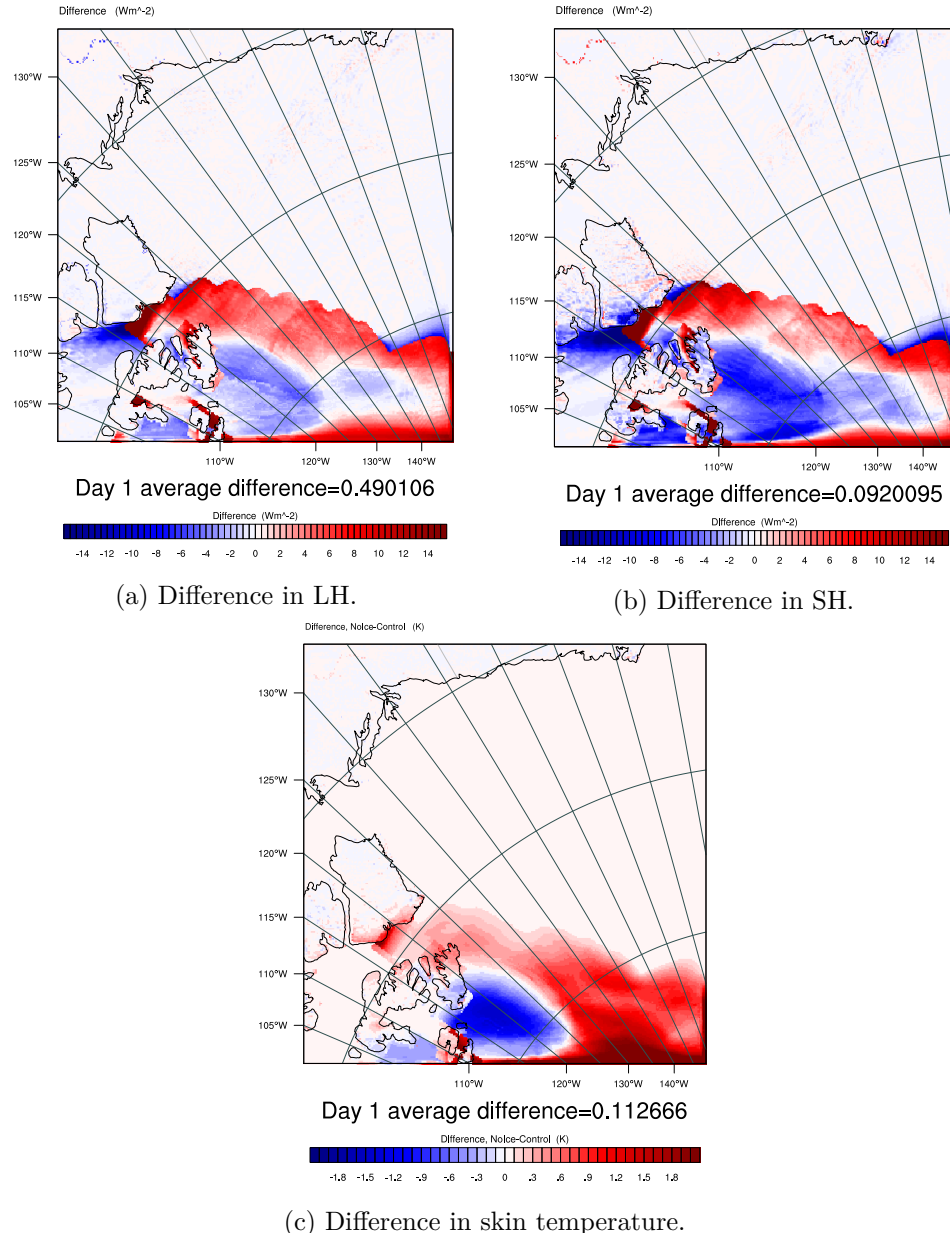


Figure 4.9: Average difference in LH, SH and skin temperature for day1. NoIce-Control.

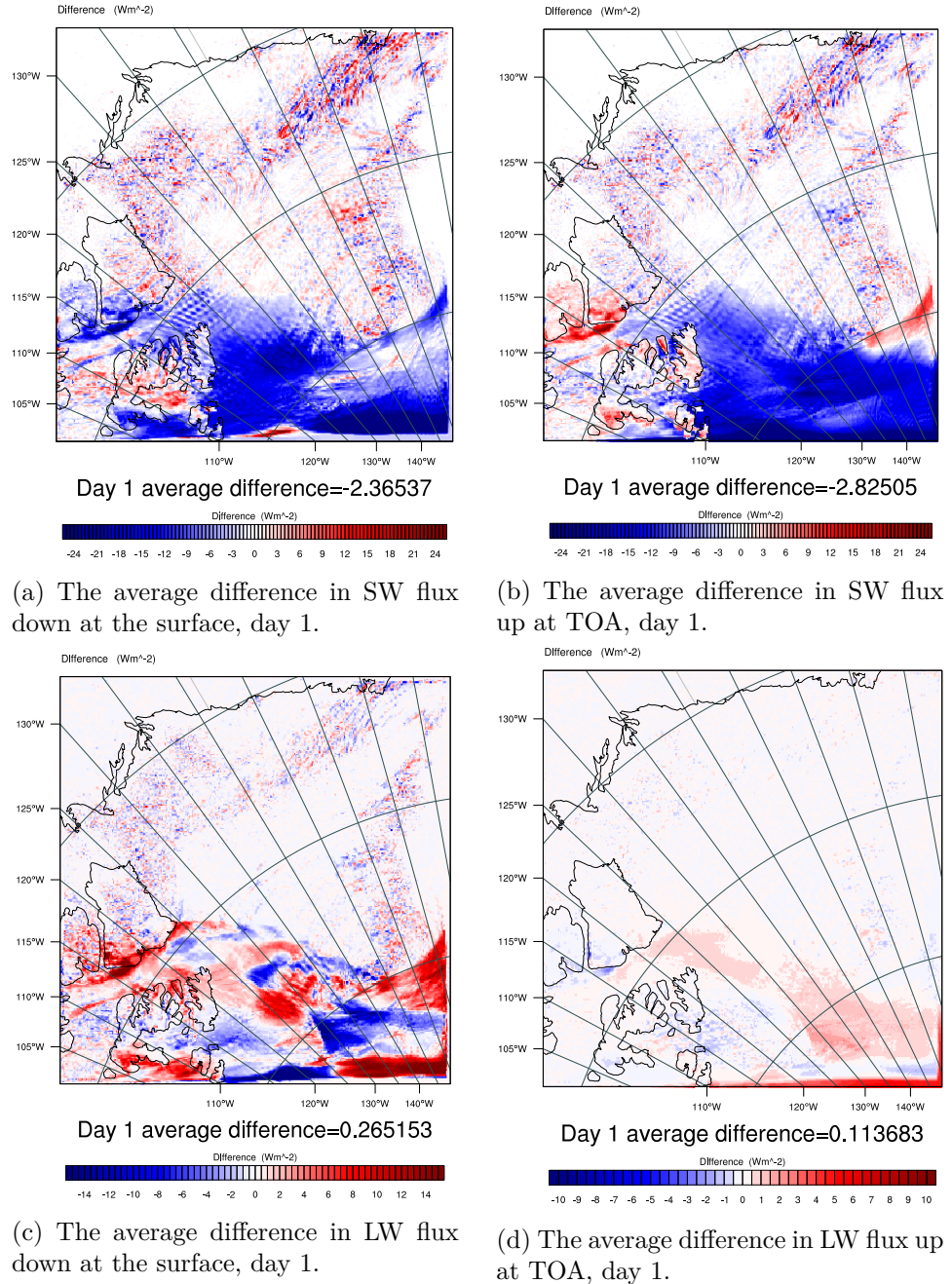


Figure 4.10: The average difference in SW and LW flux down at the surface and up at TOA, for day 1. NoIce-Control.

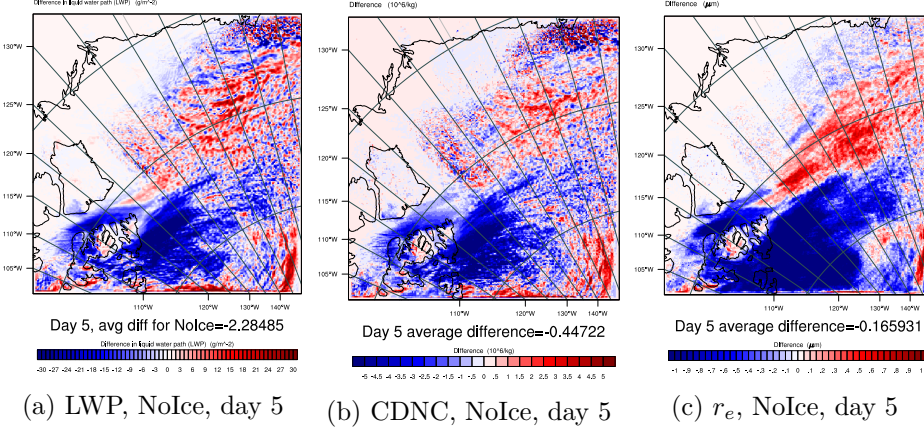


Figure 4.11: The average difference in LWP, CDNC and r_e of cloud droplets (from left to right) over the lowermost 11 layers for day 1. NoIce-Control.

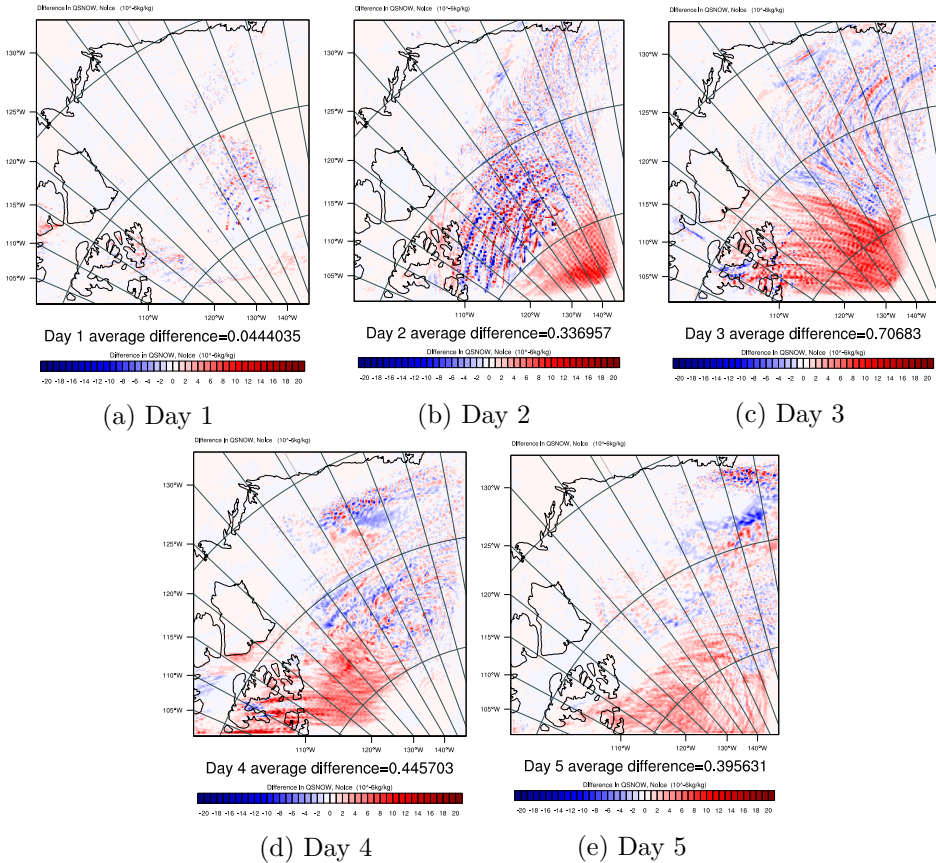


Figure 4.12: The average difference in mixing ratio of snow to air, over the lowermost 11 layers for days 1 to 5. NoIce-Control.

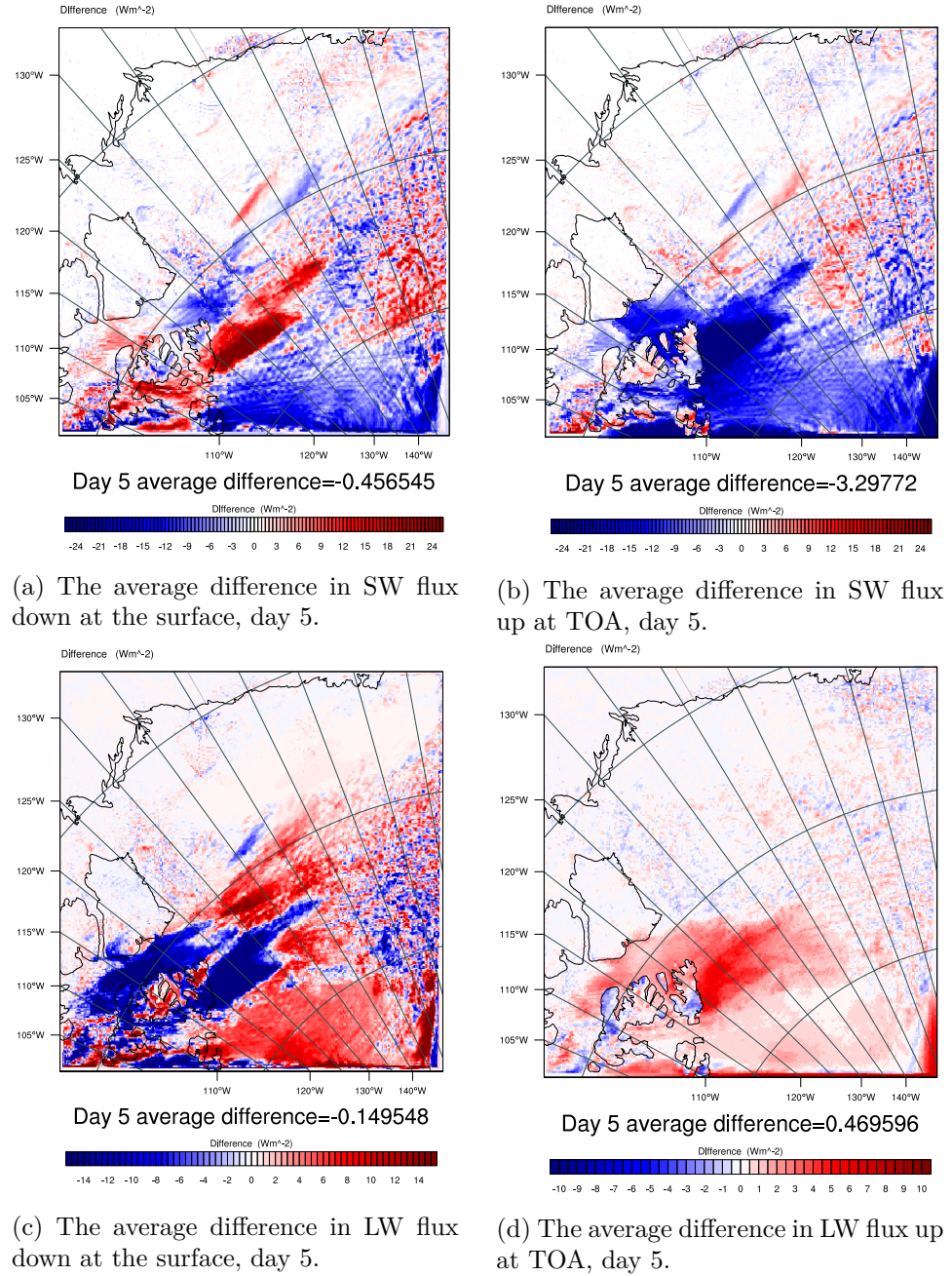


Figure 4.13: The average difference in SW and LW flux down at the surface and up at TOA, for day 5. NoIce-Control.

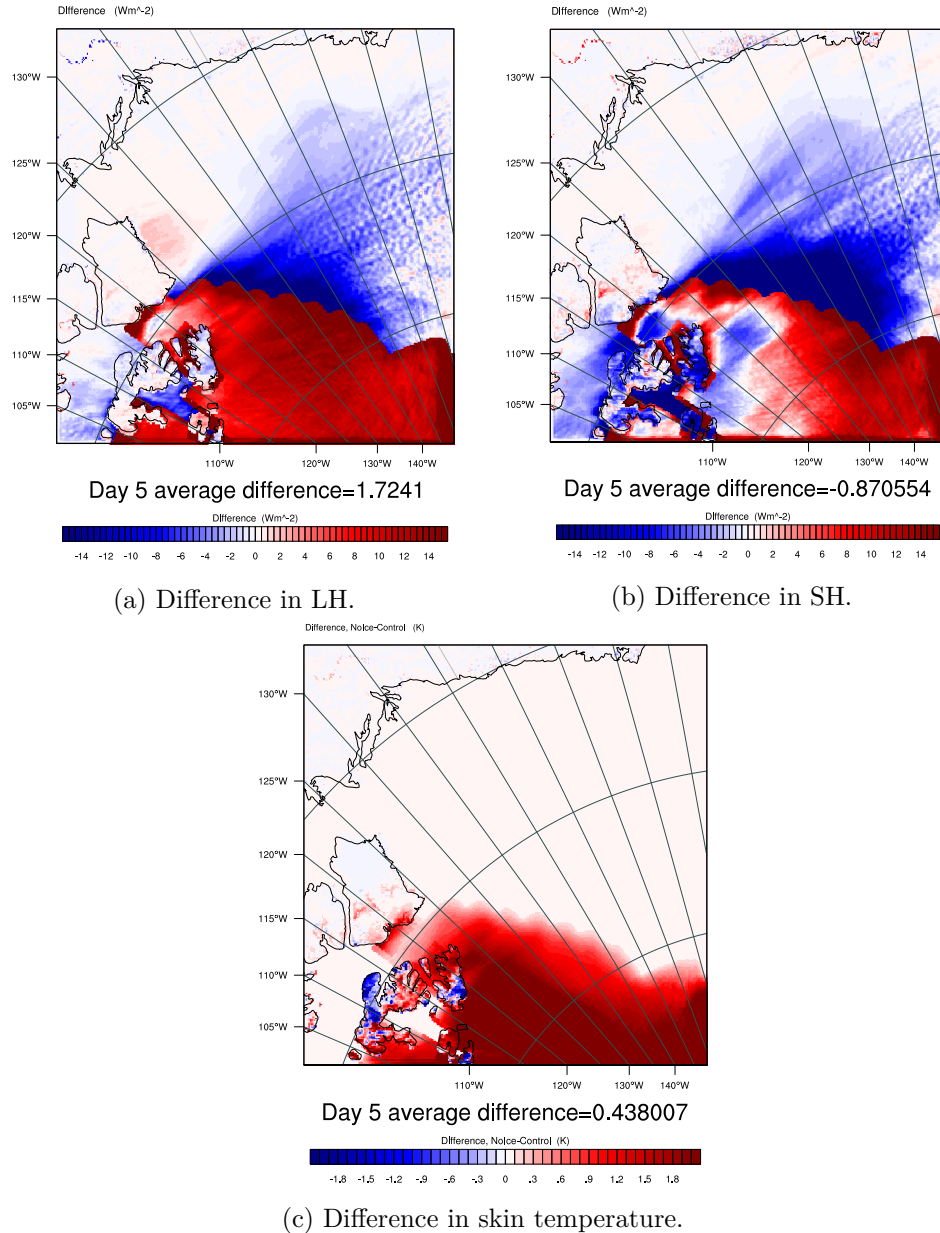


Figure 4.14: Average difference in LH, SH and skin temperature for day 5. NoIce-Control.

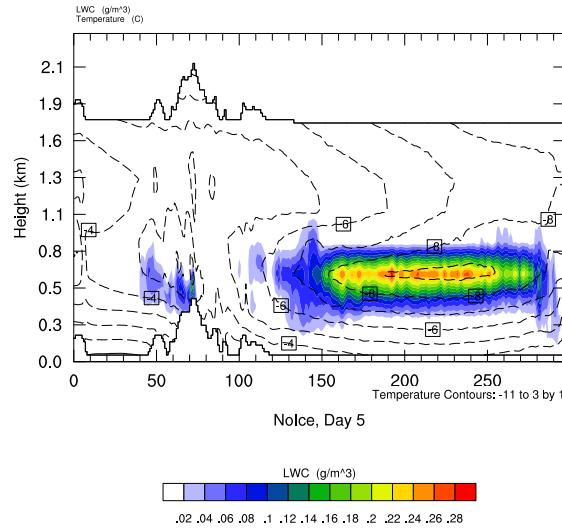


Figure 4.15: Averaged LWC in the NoIce run for day 5, in the vertical cross section over the red line in figure 4.2d.

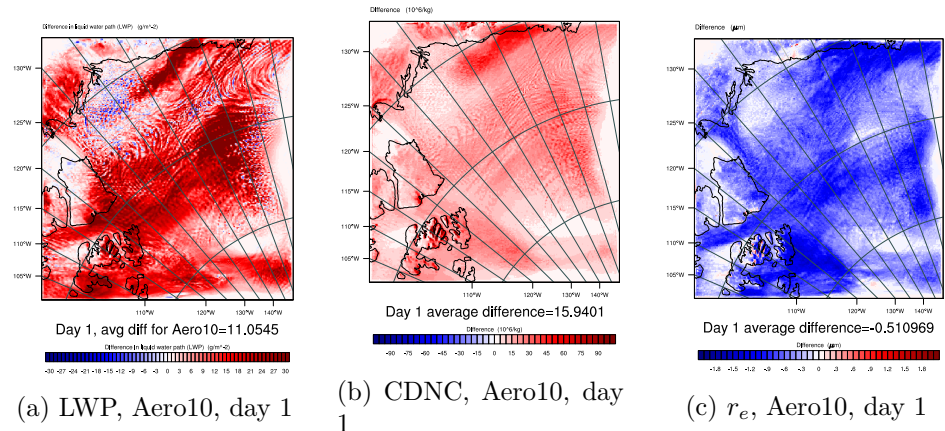


Figure 4.16: The averaged difference in LWP, CDNC and r_e of cloud droplets (from left to right) over the lowermost 11 layers for day 1. Aero10-Control.

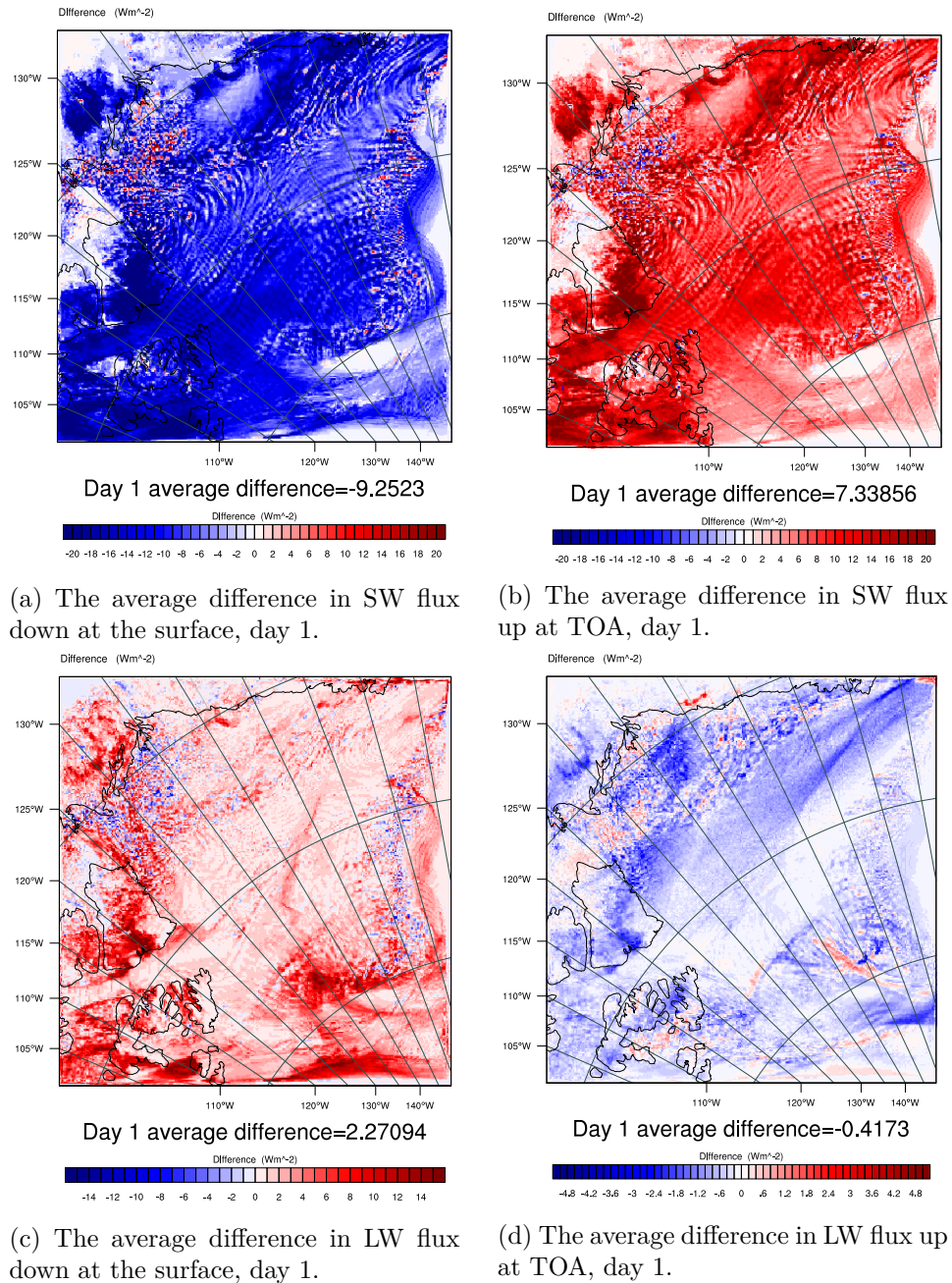


Figure 4.17: The average difference in SW and flux down at the surface and up at TOA, for day 1. Aero10-Control.

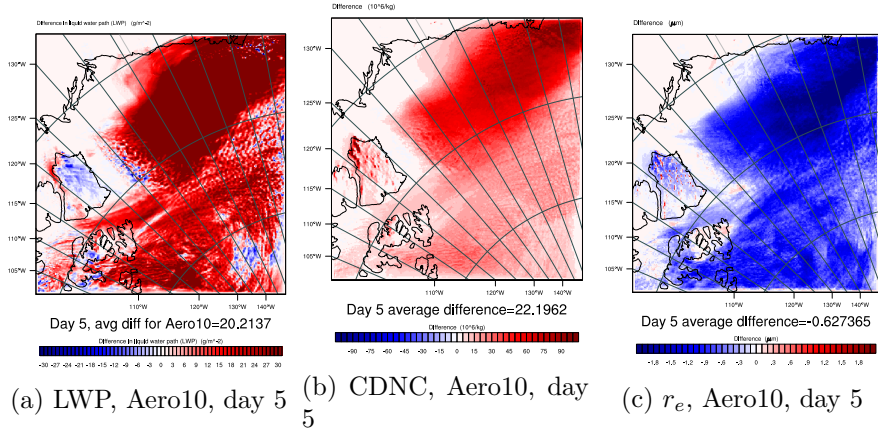


Figure 4.18: The averaged difference in LWP, CDNC and r_e of cloud droplets (from left to right) for the run with increased aerosol number concentration by a factor of 10 minus the control run, over the lowermost 11 layers for day 5.

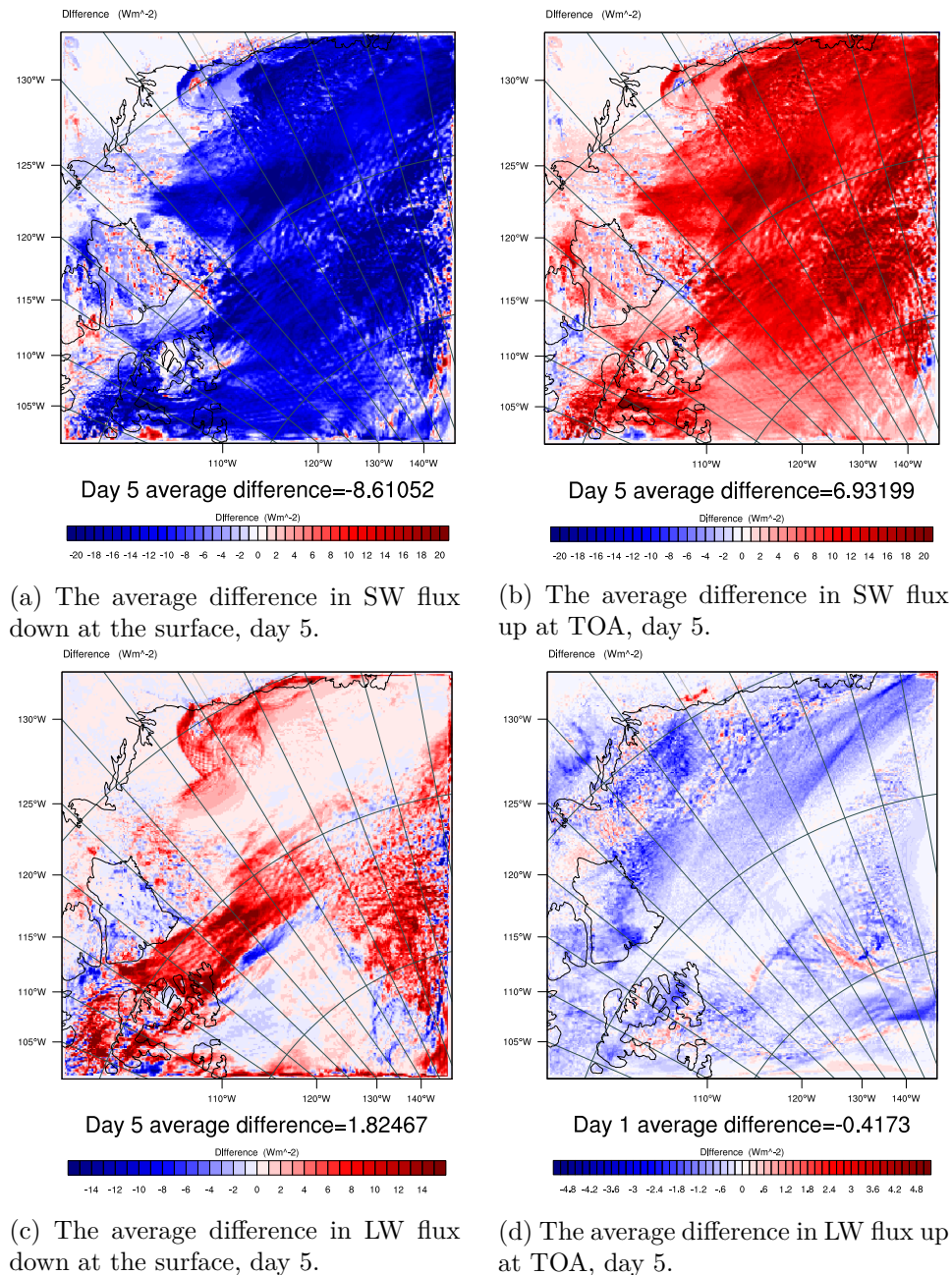


Figure 4.19: The average difference in SW and LW flux down at the surface and up at TOA, for day 5. Aero10-Control.

Chapter 5

Summary and Conclusions

In this thesis the cloud radiative response to removal of sea ice and increased aerosol number concentration was studied by use of the ARW model. The model was run over 5 days in early autumn, with and without sea ice, and with and without increased aerosol number concentration. The hypothesis was that there could be a positive feedback between the declining areal Arctic sea ice extent (eg. @ cite NSIDC) and radiative response of low Arctic stratus in autumn. Studies by @ (cite some) have found that the lack of sea ice in early autumn have led to an increase in low cloud amount. @ someone also found that the clouds had longer lifetimes when there was no sea ice beneath, due to the enhanced evaporation. @ these studies did not look at the microphysical changes in the clouds, which has been the focus of this study. The response of clouds to removal of sea ice and increased aerosol number concentration has been studied both separately and combined, for both the the first day of the run, which acts almost as an off-line run, and the last day of the run, when the atmosphere has had time to adapt to the changes implemented on the start of the first day.

Stuff to do:

- Kort oppsummering av hva som er gjort og hvorfor
- Kort oppsummering av resultater
- Kort tolkning av resultatene
- Sluttord (f.eks. videre forskning eller annet perspektiv)

Bibliography

- Aguado, Edward, & Burt, James E. 2010. *Understanding Weather and Climate*. 5th edn. Pearson Prentice Hall.
- Albrecht, Bruce A. 1989. Aerosols, Cloud Microphysics, and Fractional Cloudiness. *Science*, **245**(4923), 1227–1230.
- Beitler, Jane. 2012. Arctic sea ice extent settles at record seasonal minimum. *National Snow and Ice Data Centre U.S.A.*
- Boucher, O., Randall, David, Artaxo, P., Bretherton, C., Feingold, G., Forster, P., Kerminen, V.M., Kondo, Y., Liao, H., Lohmann, U., Rasch, P., Satheesh, S. K., Sherwood, S., Stevens, B., & Zhang, X. Y. 2013. Clouds and Aerosols. *Pages 571–657 of:* Stocker, T. F., Qin, D., Plattner, G.-K., Tignor, M., Allen, S.K., Boschung, J., Nauels, A., Xia, Y., Bex, V., & Midgley, P. M. (eds), *Climate Change 2013: The physical Science Basis. Contribution of Working Group I to the Fifth Assessment Report of the Intergovernmental Panel on Climate Change*. Cambridge University Press, Cambridge, United Kingdom and New York, NY, USA.
- Curry, J. a., Hobbs, P. V., King, M. D., Randall, D. a., Minnis, P., Isaac, G. a., Pinto, J. O., Uttal, T., Bucholtz, A., Cripe, D. G., Gerber, H., Fairall, C. W., Garrett, T. J., Hudson, J., Intrieri, J. M., Jakob, C., Jensen, T., Lawson, P., Marcotte, D., Nguyen, L., Pilewskie, P., Rangno, A., Rogers, D. C., Strawbridge, K. B., Valero, F. P J, Williams, a. G., & Wylie, D. 2000. FIRE arctic clouds experiment. *Bulletin of the American Meteorological Society*, **81**(1), 5–29.
- Curry, Judith A., Schramm, Julie L., Rossow, William B., & Randall, David. 1996. Overview of Arctic Cloud and Radiation Characteristics. *Journal of Climate*, **9**(8), 1731–1764.
- Eastman, Ryan, & Warren, Stephen G. 2010a. Arctic cloud changes from surface and satellite observations. *Journal of Climate*, **23**(15), 4233–4242.
- Eastman, Ryan, & Warren, Stephen G. 2010b. Interannual variations of arctic cloud types in relation to sea ice. *Journal of Climate*, **23**(15), 4216–4232.

- Graversen, Rune G, Mauritsen, Thorsten, Tjernström, Michael, Källén, Erland, & Svensson, Gunilla. 2008. Vertical structure of recent Arctic warming. *Nature*, **451**(7174), 53–56.
- Hansen, J. E., & Travis, L. D. 1974. Light scattering in planetary atmospheres. *Space Science Reviews*, **16**(1957), 527–610.
- Hobbs, Peter V. 1993. *Aerosol-Cloud-Climate Interactions*. Academic Press.
- Iacono, Michael J. 2003. Evaluation of upper tropospheric water vapor in the NCAR Community Climate Model (CCM3) using modeled and observed HIRS radiances. *Journal of Geophysical Research*, **108**(D2).
- Iacono, Michael J., Mlawer, Eli J., Clough, Shepard a., & Morcrette, Jean-Jacques. 2000. Impact of an improved longwave radiation model, RRTM, on the energy budget and thermodynamic properties of the NCAR community climate model, CCM3. *Journal of Geophysical Research*, **105**(D11), 14873.
- Iacono, Michael J., Delamere, Jennifer S., Mlawer, Eli J., Shephard, Mark W., Clough, Shepard a., & Collins, William D. 2008. Radiative forcing by long-lived greenhouse gases: Calculations with the AER radiative transfer models. *Journal of Geophysical Research: Atmospheres*, **113**(13), 2–9.
- Intrieri, J M, Shupe, M D, Uttal, T, & Mccarty, B J. 2002a. An annual cycle of Arctic cloud characteristics observed by radar and lidar at SHEBA. *Journal of Geophysical Research*, **107**(C10).
- Intrieri, J. M., Fairall, C. W., Shupe, M. D., Persson, P. Ola G, Andreas, E. L., Guest, P. S., & Moritz, R. E. 2002b. An annual cycle of Arctic surface cloud forcing at SHEBA. *Journal of Geophysical Research*, **107**(C10), 1–14.
- Kay, Jennifer E., & Gettelman, Andrew. 2009. Cloud influence on and response to seasonal Arctic sea ice loss. *Journal of Geophysical Research D: Atmospheres*, **114**(18).
- Klein, S. A., & Hartmann, D. L. 1993. The seasonal cycle of low stratiform clouds. *Journal of Climate*, **6**, 1587–1606.
- Liou, K. N. 1992. *Radiation and Cloud Processes in the Atmosphere*. Oxford University Press.
- Liou, K. N. 2002. *An Introduction to Atmospheric Radiation*. 2nd edn. Academic Press.
- Lohmann, U., & Feichter, J. 2005. Global indirect aerosol effects: a review. *Atmospheric Chemistry and Physics Discussions*, **4**(6), 7561–7614.

- Martin, G. M., Johnson, D. W., & Spice, A. 1994. The Measurement and Parameterization of Effective Radius of Droplets in Warm Stratocumulus Clouds. *Journal of the Atmospheric Sciences*, **51**(13), 1823–1842.
- McDonald, James E. 1958. *The Physics of Cloud Modification*.
- Mlawer, Eli J., Taubman, Steven J., Brown, Patrick D., Iacono, Michael J., & Clough, Shepard a. 1997. Radiative transfer for inhomogeneous atmospheres: RRTM, a validated correlated-k model for the longwave. *Journal of Geophysical Research*, **102**(D14), 16663.
- NSIDC. 2015. *National Snow and Ice Data Center*.
- Palm, Stephen P., Strey, Sara T., Spinhirne, James, & Markus, Thorsten. 2010. Influence of Arctic sea ice extent on polar cloud fraction and vertical structure and implications for regional climate. *Journal of Geophysical Research*, **115**(D21), D21209.
- Reisner, J., Rasmussen, R M, & Bruintjes, R T. 1998. Explicit forecasting of supercooled liquid water in winter storms using the MM5 mesoscale model. *Quarterly Journal of the Royal Meteorological Society*, **124**(548), 1071–1107.
- Rogers, R. R., & Yau, M. K. 1989. *A Short Course in Cloud Physics*. 3rd edn. Butterworth-Heinemann.
- Schweiger, Axel J., Lindsay, Ron W., Vavrus, Steve, & Francis, Jennifer A. 2008. Relationships between Arctic Sea Ice and Clouds during Autumn. *Journal of Climate*, **21**(18), 4799–4810.
- Shupe, Matthew D., & Intrieri, Janet M. 2004. Cloud radiative forcing of the Arctic surface: The influence of cloud properties, surface albedo, and solar zenith angle. *Journal of Climate*, **17**(3), 616–628.
- Skamarock, W.C., Klemp, J.B., Dudhia, J., Gill, D.O., Barker, D.M., Duda, M.G., Huang, X.-Y., Wang, W., & Powers, J.G. 2008. A Description of the Advanced Research WRF Version 3. *Technical Report*, 113.
- Skamarock, William C., & Klemp, Joseph B. 2008. A time-split nonhydrostatic atmospheric model for weather research and forecasting applications. *Journal of Computational Physics*, **227**(7), 3465–3485.
- Stevens, Bjorn, & Feingold, Graham. 2009. Untangling aerosol effects on clouds and precipitation in a buffered system. *Nature*, **461**(7264), 607–613.

- Stevens, Björn, & Seifert, Axel. 2008. Understanding macrophysical outcomes of microphysical choices in simulations of shallow cumulus convection. *Journal of the Meteorological Society of Japan*, **86A**(August 2006), 143–162.
- Thompson, Gregory, & Eidhammer, Trude. 2014. A study of aerosol impacts on clouds and precipitation development in a large winter cyclone. *Journal of the Atmospheric Sciences*, 140507124141006.
- Thompson, Gregory, Rasmussen, Roy M., & Manning, Kevin. 2004. Explicit Forecasts of Winter Precipitation Using an Improved Bulk Microphysics Scheme. Part I: Description and Sensitivity Analysis. *Monthly Weather Review*, **132**, 519–542.
- Thompson, Gregory, Field, Paul R., Rasmussen, Roy M., & Hall, William D. 2008. Explicit Forecasts of Winter Precipitation Using an Improved Bulk Microphysics Scheme. Part II: Implementation of a New Snow Parameterization. *Monthly Weather Review*, **136**, 5095–5115.
- Twomey, S. 1974. Pollution and the Planetary Albedo. *Atmospheric Environment*, **8**, 1251–1256.
- Twomey, S. 1977. The Influence of Pollution on the Shortwave Albedo of Clouds. *Journal of the Atmospheric Sciences*, **34**, 1149–1152.
- Uttal, Taneil, Curry, Judith a., Mcphee, Miles G., Moritz, Donald K. Perovich Richard E., Maslanik, James a., Guest, Peter S., Stern, Harry L., Moore, James a., Turenne, Rene, Heiberg, Andreas, Serreze, Mark. C., Wylie, Donald P., Persson, Ola G., Paulson, Clayton a., Halle, Christopher, Morison, James H., Wheeler, Patricia a., Makshtas, Alexander, Welch, Harold, Shupe, Matthew D., Intrieri, Janet M., Stamnes, Knut, Lindsey, Ronald W., Pinkel, Robert, Pegau, W. Scott, Stanton, Timothy P., & Grenfeld, Thomas C. 2002. Surface heat budget of the Arctic Ocean. *Bulletin of the* ..., 255–276.
- Vavrus, Steve, Holland, Marika M., & Bailey, David A. 2010. Changes in Arctic clouds during intervals of rapid sea ice loss. *Climate Dynamics*, **36**, 1475–1489.
- Verlinde, J., Harrington, J. Y., McFarquhar, G. M., Yannuzzi, V. T., Avramov, a., Greenberg, S., Johnson, N., Zhang, G., Poellot, M. R., Mather, J. H., Turner, D. D., Eloranta, E. W., Zak, B. D., Prenni, a. J., Daniel, J. S., Kok, G. L., Tobin, D. C., Holz, R., Sassen, K., Spangenberg, D., Minnis, P., Tooman, T. P., Ivey, M. D., Richardson, S. J., Bahrmann, C. P., Shupe, M., DeMott, P. J., Heymsfield, a. J., & Schofield, R. 2007. The mixed-phase arctic cloud experiment. *Bulletin of the American Meteorological Society*, **88**(2), 205–221.

- Wallace, John M., & Hobbs, Peter V. 2006. *Atmospheric Science, An Introductory Survey*. 2nd edn. Academic Press.
- Wang, Wei, Brûyère, Cindy, Duda, Michael, Dudhia, Jimy, Gill, Dave, Kavulich, Michael, Keene, Kelly, Lin, Hui-Chuan, Michalakes, John, Rizvi, Syed, Zhang, Xin, Berner, Judith, & Smith, Kate. 2015. *WRF ARW Version 3 Modeling System User's Guide*. Mesoscale & Microscale Meteorology Division, National Centre for Atmospheric Research.
- Wu, Dong L., & Lee, Jae N. 2012. Arctic low cloud changes as observed by MISR and CALIOP: Implication for the enhanced autumnal warming and sea ice loss. *Journal of Geophysical Research: Atmospheres*, **117**(D7).